Stanev, E.V.; Kandilarov, R.:

Sediment dynamics in the Black Sea: numerical modelling and remote sensing observations

In: Ocean Dynamics (2012) Springer

DOI: 10.1007/s10236-012-0520-1

Sediment Dynamics in the Black Sea: Numerical Modelling and Remote Sensing Observations

Emil V. Stanev[1,2], and Rostislav Kandilarov[2,3]

1: Institute for Coastal Research, HZG, Max-Planck-Strasse 1, 21502 Geesthacht, Germany
2: Department of Meteorology and Geophysics, University of Sofia, James Bourchier Street, 5, 1126 Sofia, Bulgaria
3: Institute for Chemistry and Biology of the Sea (ICBM), University of Oldenburg, Carl-von-Ossietzky-Strasse 9-11, D-26111 Oldenburg, Germany

Keywords: Sediment Transport,TSM, SPM, Numerical Modelling, Remote Sensing, Black Sea

Contents

List of Figures

List of Tables

Abstract

Here, we address the sediment dynamics in the Black Sea based on analysis of remote sensing data from MERIS satellite spectrometer and numerical simulations with NEMO model. Boundary conditions consist of realistic meteorological forcing, including significant wave height generated by WAM model. A number of sensitivity runs was analysed with the aim to find the most suitable parameters governing sediment fluxes. The comparison between numerical simulations and remote sensing data gives credibility to the quality of simulations. The combined effect of wind waves and currents in the bed layer controls the sediment resuspension that appears to be the major basin wide source of sediment. Sensitivity experiments included or excluded different forcing terms, e. g. sediment flux from rivers enable to determine the spatial extensions of different point-sources. It is concluded that wind-wave forcing is manifested in the sediment dynamics through episodic high energy events contributing to the increase of horizontal sediment fluxes over the north-western shelf. Both satellite images and numerical model simulations demonstrated that the penetration of suspended sediment into the basin interior is governed by the dynamics of coastal and open-ocean eddies. While fine sediment at sea surface could cross the continental slope extending into the open ocean, coarser fractions follow the bottom and their penetration into the open ocean is limited. The conclusion is thus that the deposition patterns correlate with the specific shape of Black Sea topography largest depositions are observed in the area of continental slope. Analysis of numerical simulations could motivate further observations aiming to verify the possibility identified in the numerical simulations that winter convection/mixing could also affect the propagation of fine suspended sediment.

1 Introduction

The Black Sea is a nearly enclosed deep basin connected to the Sea of Marmara and the Sea of Azov by the narrow Bosporus and Kerch Straits, respectively (figure 1). The area shallower than 200 m (light blue area, which gives 27 percent of the total area), is mainly located in the northwest. Black Sea catchment area of about 1,864,000 km^2 covers large parts of Europe and Asia (figure 1), providing a total freshwater supply of $3 \times 10^2 km^3$ per year. This large amount of fresh water flux along with the narrow opening in the strait of Bosporus make the Black Sea a typical estuarine basin where the surface salinity is about half that of the Mediterranean's. The strong vertical (haline) stratification limits the vertical exchange and creates a unique chemical and biological environment.

The circulation in the Black Sea is structured in two connected gyre systems called Eastern and Western Gyres encompassing the basin (the Rim Current, figure 2). This is a frontal current associated with a difference of $\sim$0.2 m between sea level in the coastal and open sea. Its position is controlled by the bottom topography, which is characterised by a gentle slope in the northwestern and western Black Sea and abrupt one along the southern and eastern coasts (see the contrast between light blue and dark blue areas in figure 1). Anticyclonic eddies are formed between the Rim Current and the coast, the most prominent of them are the Batumi and Sevastopol eddies (figure 2)

Annual production of organic mater of 818×10^6t yr^{-1} exceeds substantially the total sediment load from the rivers around the Black Sea periphery of about 150×10^6t yr^{-1} (figure 3, see also Shimkus and Trimonis, 1974; Panin and Jipa, 2002; Balkas et al., 1990; Bondar et al., 1991; Panin, 1996). About 65 percent of this amount enters into the northwestern shelf region (Hay, 1994). The sedimentary and ecological systems of the continental shelf are dominated by the fluxes from the major rivers, the Danube, the Dniester, and the Dnieper (Oguz, 2005). The River Danube, which accounts for $\sim$ 60 percent of the total river input into the northwestern continental shelf discharges 45 to 50×10^6t yr^{-1} of suspended solids into the Black Sea (Popa 1993). The Danube Delta is subjected to waves primarily approaching from the east, driving net sediment transport towards the southwest (Giosan et al., 1999; Giosan et al., 2005). Under some specific circulation conditions (Stanev et al., 2002) the

Danube plume is entrapped by an anticyclonic shelf-gyre extending to the north. Average sedimentation rates for the Upper Quaternary range between 1.19 and 2.19 m ka $^{-1}$ for the Danube fan and between 1.07 and 2.03 m ka $^{-1}$ for the Dnieper fan (Winguth et al., 2000). These values are much higher than in other Mediterranean basins, which is caused by the large drainage area of the Black Sea. The thickness of sediment layers that have accumulated over the last 3000 years of the Black Sea history is 20 to 80 cm depending on the region. Sediment trap data (Hay and Honjo, 1989) reveal large variations in the total particle flux (from 2 to 71 mg $m^{-2}day^{-1}$). Fine-grained terrigenous matter may remain in suspension in the surface water for several months, which may be a sufficient time to transport the suspended matter across the basin before it settles to the sea floor.

The sediment pattern in the near-shore zone of the Black Sea is governed by the surface and alongshore bottom currents and wave action (Ross et al., 1978; Nikolov et al., 2006). In the western Black Sea suspended particulate mater (SPM) from the Danube, Dnieper, and other big rivers is deposited and trapped on the broad western shelf. In the eastern basin, the terrigenous material easily crosses the narrow shelf and enters the deep basin.

SPM is also referred to as Total Suspended Mater (TSM) in the literature and we will use here the two abbreviations as synonyms. SPM in the Black Sea has terrestrial, planktonic, bacterial and fossil origin. Grain size fraction $< 2\mu m$ is characteristic for the abyssal plane, 6.3-20 μm for the slope area and $20 - 63\mu m$ for the shelf, but also for the slope area (Müller and Stoffers, 1974). According to Wakeham et al. (1991) the vertical profile of TSM displays high concentrations in surface waters ($\sim 400\mu g/l$ at 2 m), which decreases to $\sim 150\mu g/l$ at 200 m and does not change much down to 1000 m (figure 4). Noteworthy is that TSM gives the overall picture of sediment distribution, which includes also plankton ($< 63\mu m$), the later is dominant in the interior Black Sea. The separation between TSM of different origin is a difficult issue, also when one analyses satellite data (see further in the text).

Recent remote sensing data contributed to further understanding of the basin-wide sediment dynamics and provided valuable material for the validation of numerical models. Sur et al. (1996) used satellite (CZCS, AVHRR) and in-situ (CTD, ADCP) data to characterise the impact of meso-scale motions and boundary currents on the transport and productivity along the wide Western Black Sea shelf. They found

various forms of isolated transient features such as filaments, coherent dipole and monopole eddies, and jets to contribute substantially to the transport of SPM across the continental shelf.

Karabashev et al. (2006) demonstrated the potential of SeaWiFS imagery (figure 5) to describe the horizontal patterns (vortex dipoles) associated with the coastal/deep basin water exchange. Their remote sensing data indicated that the patterns are influenced by sediments from the Danube Delta. Similar patches and filaments were observed earlier in the same area by Ginzburg et al. (1997) and Guneroglu et al. (2005).

Kopelevich et al. (2004) analysed the spatial and temporal variability of the bio-optical characteristics in the Black Sea derived from SeaWiFS data in 1998 - 2001 and concluded that fluvially derived particles are spread over the entire basin. The particulate matter brought by the rivers in the northwestern part (mainly by the Danube River) is transported along the coast by the Rim Current and across the shelf-continental slope area by meso-scale eddies and via turbulent exchange (see, as an example, their Fig. 12).

Unlike to observations, numerical modelling of sediment transport in the Black Sea is still underdeveloped, differently from the case of the neighboring Mediterranean Sea where several good examples already exist (Wang and Pinardi, 2002; Kourafalou et al., 2004; Sherwood et al., 2004; Ulses et al., 2008; Harris et al., 2008, Bevera et al., 2009) demonstrating very promising results. It has been established in these studies that the wave-induced remobilisation of the deposits is a key mechanism of cross-shelf sediment transport (see also Traykovski et al., 2000). To our knowledge, the only experience existing in the field of numerical modelling of (coarse) sediment in the Black Sea is due to Giosan et al. (2005), who address the morphodynamics of the wave-influenced Danube Delta.

The motivation of this study is to initiate first steps toward development of basin scale modelling capabilities for sediment transport in the Black Sea. Because we address the entire basin, we include in our numerical simulations not only coarse, but also fine sediment fractions which could propagate far from their river and bottom origin and sometimes penetrate the basin interior. Evaluating geomorphic evolution or delta growth is not addressed in the present study, neither the bed-load transport. Dealing with fine sediment leads to a substantial difficulty, which is the

separation between sediment from rivers and sediment remobilized from bottom, from one side, from the sediment due to biological productivity, from the other. Modelling approach to this problem would necessitate using coupled biological and sediment models with an appropriate description of the processes associated with the interaction of these two kinds of sediment and grain size variation. Further in this direction is the issue of simulating optical properties affecting biological productivity. The present study, which could be considered as a first step, does not consider the biogeochemistry, therefore the research questions addressed are limited to physical processes and aim to: (1) present a sediment transport model for the Black Sea, (2) demonstrate the realism of simulations, mainly through comparison with remote sensing data, (3) learn more about the Black Sea sediment dynamics. One additional motivation of this study is to identify some important problems in sediment modelling in the Black Sea and, based on solved and unsolved problems, to formulate the direction of future steps in this field. Following these lines we first describe the numerical model in section 2, followed by the analysis of results in section 3 and conclusions.

2 Models and data

2.1 Brief description of the model

Circulation model

Extended references on numerical modelling of the Black Sea circulation are provided in several reviews (Stanev, 1990; Stanev et al., 2002; Kara et al., 2005, Stanev, 2005). Although there are many models used so far, one relatively new one Nucleus for European Modelling of the Ocean (NEMO) (Madec, 2008) deserves our attention, therefore, we describe here very briefly its setup for the Black Sea (for more details see Grayek et al., 2010). The appropriate resolution of important physical processes, rich physical parametrisations, and conservation properties justify our selection of this model.

The NEMO is discretized on an Arakawa C grid. The horizontal resolution in our Black Sea setup is $1/12^{\circ}$, thus, we have a matrix of 133x76 points, which is the same as in our similar previous works based on the Modular Ocean Model

(MOM) setup for the Black Sea (Stanev et al., 2003). The investigated area extends from $27°38'E \times 40°45'$N to $42°05'$E $\times$ $46°70'$N. The vertical grid uses a hard-wired hyperbolic tangent stretching function with 31 levels. Our setup employs also partial step representation of bottom topography (Barnier et al., 2006) in order to adjust the model depth to the observed one.

For lateral mixing of tracers (temperature, salinity and sediment) we use a second-order geopotential operator (Laplacian) with $A^{lT} = 100\mathrm{m}^2\mathrm{s}^{-1}$, where indices "$l$" and "$T$" stay for "lateral" and "tracer", correspondingly. A geopotential bi-laplacian operator (Griffies, 2004) parametrizes the horizontal eddy viscosity with A^{lm} = -7 $\times$ $10^9\mathrm{m}^4\mathrm{s}^{-1}$, where "m" stays for "momentum". The vertical (index "v") eddy viscosity A^{vm} and diffusivity A^{vT} coefficients are computed from a closure scheme (Madec, 2008) with a prognostic equation for the turbulent kinetic energy $\overline{e}$ and a closure assumption for the turbulent length scales, so that the time evolution of $\overline{e}$ is a result of its production through vertical shear, destruction through stratification, vertical diffusion, and dissipation:

$$\begin{aligned} \frac{\partial \overline{e}}{\partial t} = A^{vm}\left[(\frac{\partial u}{\partial z})^2 + (\frac{\partial v}{\partial z})^2\right] &- A^{vT}N^2 + \frac{\partial}{\partial z}\left[A^{vm}\frac{\partial \overline{e}}{\partial z}\right] - c_\epsilon \frac{\overline{e}^{3/2}}{l_\epsilon} \\ A^{vm} &= C_k l_k \sqrt{\overline{e}} \\ A^{vT} &= A^{vm}/P_{rt} \end{aligned} \tag{1}$$

where u and v are the horizontal velocity components, N is the local Brunt-Vaisala frequency, l_k and l_ϵ are the dissipation and mixing length scales, P_{rt} is the Prandtl number, $C_k = \sqrt{2}/2$ and $C_\epsilon = 0.1$. In addition, an enhanced vertical diffusion is applied on both tracer and momentum which means assigning large value A^{vT}_{max} = $A^{vm}_{max} = 1\ \mathrm{m}^2\mathrm{s}^{-1}$ to the vertical eddy diffusivity coefficients in regions with unstable stratification, whereas their minimal values are set to be $A^{vT}_{min} = 1.2 \times 10^{-5}\mathrm{m}^2\mathrm{s}^{-1}$ and $A^{vm}_{min} = 1.2 \times 10^{-4}\mathrm{m}^2\mathrm{s}^{-1}$. The selected advection scheme for tracers is the total variation diminishing (TVD) scheme, which is, at best, second-order accurate (Barnier et al., 2006). TVD scheme may be viewed as a nonlinear flux limiter that adds just enough diffusion to prevent numerical instabilities.

Sediment transport model

The sediment transport model uses a standard diffusion-advection equation (the same as for the temperature and salinity) for the SPM concentration c with an extra sinking term added on the right hand side:

$$\frac{\partial c}{\partial t} + u\frac{\partial c}{\partial x} + v\frac{\partial c}{\partial y} + w\frac{\partial c}{\partial z} = A^{lT}\Delta c + \frac{\partial}{\partial z}\left(A^{vT}\frac{\partial c}{\partial z}\right) + \frac{\partial}{\partial z}\left(w_s c\right) \tag{2}$$

where w is the vertical velocity component and w_s is the settling velocity of the sediments in suspension. Here we refer to these particles as to mud or fine SPM ($d < 63\mu m$) and we assume that they are non-cohesive (do not flocculate or aggregate) and that their concentration (relatively small) has no effect on the water density.

Deposition and erosion

Deposition and erosion rates are controlled by the bed shear stress $\tau_b = A^{vm}(\partial u/\partial z)$. The sediment flux at the sea bed is

$$\left(A^{vT}\frac{\partial c}{\partial z}\right)_{z=H} = \begin{cases} -D & \tau_b < \tau_d \\ E & \tau_b > \tau_e \end{cases} \tag{3}$$

where D and E are deposition and erosion rates. Deposition rate given by Einstein and Krone (1962) is

$$D = w_s \times c_b\left(1 - \frac{\tau_b}{\tau_d}\right), \tag{4}$$

where c_b is the bottom concentration and τ_d is the critical shear stress for deposition. The definition of the bottom concentration c_b is as for the remaining (standard) tracers in NEMO, and uses the modifications associated with partial steps, connected with the fact that bottom depths do not equal the standard model depths (see Madec, 2008).

The erosion rate is computed using the formula of Partheniades (1965):

$$E = M_e\left(\frac{\tau_b}{\tau_e} - 1\right), \tag{5}$$

where M_e is an empirical parameter giving the erosion rate at twice the critical shear stress for erosion τ_e.

The critical shear stress for deposition is chosen to be equal to that for erosion: $\tau_d = \tau_e = \tau_{crit}$. This means that either deposition or erosion occurs and no region of transition exists where neither of the two processes are active. Following previous studies Wang and Pinardi (2002) we assume $\tau_{crit} = 2 \times 10^{-2} N m^{-2}$.

2.2 Model forcing, boundary conditions and experiments

The data used here to construct the forcing consists of radiation (including clouds), temperature and relative humidity at 2 m and atmospheric winds at 10m. They are produced by the European Centre for Medium-Range Weather Forecasts (ECMWF) and were kindly made available in the frame of SESAME (Southern European Seas: Assessing and Modelling Ecosystem changes) project by the INGV, Italy. The temporal sampling rate is 6 hours and the spatial resolution is $0.25° \times 0.25°$.

It is important to mention that the actual forcing in the model is derived interactively - that is the heat fluxes depend on the sea surface temperature (SST), which is a model variable. This type of forcing has been proved successful in regional ocean models of the Mediterranean (Roussenov et al, 1995) and the Black Sea (Staneva et al., 1995; Stanev at al., 2003).

A spin-up of one year forced with climatological data (mean year) has first been performed, followed by an integration for the period 2006-2009 with realistic forcing data. All experiments are forced with time-varying meteorological condition.

Momentum flux

The momentum flux in the model is introduced through the wind stress components:

$$(\tau_x, \tau_y) = \rho_a C_d |W| (W_x, W_y) \tag{6}$$

where (W_x, W_y) are the wind components at 10 m, ρ_a is the density of air and C_d is the drag coefficient, which is stability dependent (Grayek et al., 2010). This mechanical forcing is shown in figure 6a as the annual mean wind. The area mean

wind-stress curl is positive throughout the year with largest positive anomalies (cyclonic curl) located in the eastern Black Sea. Overall, the spatial pattern is consistent with the similar ones displayed by Stanev et al.(2003) and Grayek et al. (2010).

Thermohaline fluxes

Surface buoyancy forcing is controlled by thermohaline fluxes shaped by air temperature and humidity as well as precipitation. Evaporation is diagnosed in the model using bulk aerodynamic formulas. The total heat flux is

$$Q_T = Q_s - H - LE - Q_b, \tag{7}$$

where Q_s is the downward flux of solar radiation, H is the sensible heat flux, E is evaporation, L the latent heat of evaporation and Q_b is the upward flux resulting from the long wave radiation lost from the sea surface. In our model, we used the same parametrisations for the individual components of heat fluxes as in Stanev et al. (2003).

Virtual surface salinity flux is

$$Q_{sal} = Q_W S, \tag{8}$$

where $Q_W = R+P-E$ is the difference between the river runoff (R) and precipitation (P), from one side and the evaporation (E) from the other, S is the surface salinity (18 psu in the Black Sea). The approximation $S = 18psu$ in equation (8) is good except in the vicinity of Danube Delta. However, its advantage is that a globally balanced $P - E$ field converts to a globally balanced surface salinity flux (i.e., the global mean salinity in a model does not change). The salinity balance is closed in the strait of Bosporus (see further in the text).

The model has been initialised with horizontally uniform temperature and salinity profiles taken from climatological data. The geothermal heat and salinity flux at the bottom were neglected.

Fluxes from rivers and Bosporus Strait

The river runoff data used in the model (figure 7a) is based on the monthly mean data for the period 1960-2000 (Ludwig et al.,2009). The major coastal sources of

SPM are defined as point sources (river mouths) and the values are computed from the data presented by Panin and Jipa (2002, see their Table 1). The major non-point source (sink) of sediments is the sea floor.

The horizontal boundaries were closed for the Kerch Strait and open for the Bosporus Straits. This formulation follows the consensus that the transport in the Bosporus Straits is crucial for the Black Sea oceanography. As shown by Peneva et al. (2001), there is a clear correlation between the river runoff and the barotropic straits transport. Therefore, we estimated the barotropic transport in the Straits of Bosporus R_{Bo} as a linear function of the river runoff R_{ri}. The monthly variation of the water outflow R_{Bo} was constructed according to the monthly mean data $R_{ri,L}$ of Ludwig et al.(2009) with "corrected" mean value relative to the one of the annual mean climatological river runoff $R_{ri,K}$ of Kara et al. (2007, see their table 7):

$$R_{Bo} = k\left\{R_{ri,L} - \left(\overline{R_{ri,L}} - \overline{R_{ri,K}}\right)\right\} \tag{9}$$

where $\overline{(.)}$ is the annual mean and the coefficient k is found using the least mean squares method for the function $R_{Bo}(R_{ri,K})$. The inflow from the Bosporus Straits is applied in the model as "negative" river at a grid point near the shore (so that $R = R_{ri} - |R_{Bo}|$) whereas the corresponding salinity flux Q_{sal}^{Bo} is computed as in equation (8) with $S = 36psu$, which reflects Marmara Sea conditions.

Tidal processes were neglected because for the Black Sea (small and enclosed basin) tides have very small amplitude.

Bed shear stress

We represent the bed shear stress

$$\tau_b = \tau_b^c + \tau_b^w$$

as a sum of two terms: due to currents (index "c") and due to wind waves (index "w"), (Grant and Madsen, 1979; Signell et al., 1990).

The former was computed in the circulation model using quadratic friction law:

$$\tau_b^c = \rho C_{Db} U^2 \tag{10}$$

where U is the current velocity in the lowest water layer and C_{Db} is the friction coefficient at the bottom. Assuming a logarithmic current profile yields

$$C_{Db} = \left(\frac{1}{\kappa} \left(1 + ln(z_0/\Delta h)\right) \right)^{-2} \tag{11}$$

where $\kappa = 0.4$ is the Von Kármán constant, Δh is the thickness of the lowest water level and $z_0 = 2.083 \times 10^{-5} m$ is the roughness length for mean grain size of $25 \mu m$ (Gayer et al., 2006, Soulsby 1997).

The contribution of wind waves to sediment dynamics uses the well-known concept that the turbulent kinetic energy associated with wave-induced bed shear stress can be described (like in the steady flows) as proportional to the second power of the orbital velocity (Jonsson, 1966):

$$\tau_b^w = 0.5 \rho f_w U_w^2 \tag{12}$$

where U_w is the maximum of the horizontal orbital wave velocity at a water depth h. Orbital velocity can be computed from the linear wave theory assuming an equivalent sine wave for the significant wave height H_s, provided peak period T and wave number k are known as:

$$U_w = \frac{\pi H_s}{T \sinh(kh)} \tag{13}$$

The wave friction factor f_w is determined by the maximum of the rough bed friction and the smooth bed friction coefficients computed as in Gayer et al.(2006).

The wave spectra properties(H_s, T, k) are computed by WAve Prediction Model WAM - a third generation non-stationary surface wave prediction model (G.J.Komen et al, 1994, Günther et al.,1991, WAMDI Group., 1988). The horizontal resolution of WAM, the used bottom topography, as well as the surface wind were the same as those used in the circulation model, so that the waves are fully consistent with the wind (see figure 6a,b and figure 7b,c). The WAM setup is essentially the same as the one used by Gayer et al. (2006). Numerical simulations agree with the dominating consensus that the Black Sea wind waves are characterised by large seasonal variability(figure 7c), the winter storms are much more frequent than the summer ones (see also Abdalla and Ozhan, 1999; and Cherneva et al. 2008). In

the open sea winds from the North and East prevails(figure 6a), generating extreme waves coming from these directions(figure 6b‘).

Bottom distribution of SPM

To our knowledge, there is no data available Black Sea-wide like in some other ocean basins (North Sea for instance, see Gayer et al., 2006) to specify the bed properties. A naive assumption for unlimited source of SPM at the bottom would lead to an overestimation of the resuspension for both cohesive and non-cohesive sediment (Wiberg et al., 1994, Sanford and Maa, 2001). One solution to this problem is to limit the ability for resuspension at the sea floor as a function of depth in a similar way as this has been done for the Baltic Sea by Gayer et al. (2006). Formally this approach assumes that in equation (5):

$$M_e = M_e(x,y) = M_{e,b} * \theta(x,y) \tag{14}$$

so that the "background value" $M_{e,b}$ is reduced by by a topography dependent factor θ:

$$\theta(x,y) = \begin{cases} 0 & h(x,y) \leq h_{min} = 2m \\ \frac{h(x,y)-h_{min}}{h_{max}-h_{min}} & h_{min} < h(x,y) < h_{max} = 150m \\ 1 & h_{max} \leq h(x,y) \end{cases}$$

which is linearly proportional to the sea depth. The topography dependence is calibrated in a way that proposed parametrisation reduces resuspension to zero in the very shallow waters($h < h_{min} = 2m$), below $h_{max} = 150m$ $\theta = 1$. A number of sensitivity experiments was first carried out in order to ensure reasonable fluxes consistent with the distribution of bottom sediment given by Ross et al. (1978). The chosen value for the empirical parameter $M_{e,b} = 3.7 \times 10^{-7} kgm^{-2}s^{-1}$ is lower that other studies (Clarke and Elliot, 1998; Wang and Pinardi, 2002) but similar to Stanev et al. (2007) and shows good results.

2.3 Experiments

Experiment name	FSE	CSE	WCSE	RCSE
Sedimentation speed w_s [m/s]	10^{-5}	10^{-4}	10^{-4}	10^{-4}
Bed shear stress τ_b	$\tau_b^c + \tau_b^w$	$\tau_b^c + \tau_b^w$	$\tau_b^c + \tau_b^w$	τ_b^c
Sediment input from rivers	yes	yes	no	yes

Table 1: Summary of the performed experiments in this paper.

Several numerical experiments summarised in table 1 were performed. The first two analyse the transport of different types of sediments. The former - Fine Sediment Experiment(FSE) with settling velocity $w_s = 10^{-5} ms^{-1}$ represents very light sediment, which can be considered as a product of biological activity. The Coarse Sediment Experiment(CSE) is representative for heavier sediments delivered by rivers with typical sedimentation speed $w_s = 10^{-4} ms^{-1}$. The above sinking velocities are in the range of the once proposed in other similar studies (Wang and Pinardi, 2002, Gayer et al., 2006). More information about parameters describing sedimentation in other coastal seas are given in Mehta (1988), Clarke and Elliot (1998), Puls et al. (1999), Wang and Pinardi (2002), Mikkelsen et al. (2007), Milligan et al. (2007).
To analyse the significance of river discharge and resuspension from the bottom we perform two more experiments. In one of them named Wind Coarse Sediment Experiment(WCSE) sediment input from river mouths was neglected. On the contrary, in River Coarse Sediment Experiment(RCSE) the sediment flux from rivers was enabled, but the forcing associated with the wind waves was neglected.

2.4 Satellite observations and data processing

Satellite data give a valuable source of information to study temporal and spatial characteristics of TSM. The Medium Resolution Imaging Spectrometer (MERIS) which operates on the environmental remote sensing satellite ENVISAT is used to retrieve the concentrations of phytoplankton pigment, suspended matter and yellow substances ("gelbstoff") from water leaving radiance reflectance (Doerffer and Schiller, 1998; Doerffer et al., 2006). The used algorithm is a multiple non-linear regression method ("Neural Network") that needs as an input the directional water

leaving radiance reflectances of 8 MERIS bands and solar and observation angles. Its coefficients are determined using a feed forward back-propagation optimisation ("training") technique. Two key features of the presented algorithm justified its choice: (1) it treats a wide range of concentrations which cover open ocean case I water as well as turbid case II waters, and (2) it is capable to separate the suspended matter from the other substances. The Basic Toolbox for ENVISAT (A)ATSR and MERIS (BEAM)(Brockmann, 2003), provided by ESA ENVISAT project includes plugin with the latest validated version of this Neural Network. We had applied it over the raw MERIS level 1 data for 2007-2008 period to produce TSM concentration in the Black Sea (figure 11) that is to produce MERIS level 2 data.

The propagation of turbid waters and their variability in time and space was intimately related to sediment transport and remobilisation. Daily mapping of satellite data can be used to derive important statistics, observe the extension of river plumes, and the re-suspension of sediments from the bottom in shallow waters, usually due to wind-wave action. The data is available as a MERIS level 3 product generated after re-processing the MERIS level 2 data. The detection of turbid water is based on a threshold value of water reflectivity at a given wavelength of the spectrum equivalent to a sediment concentration of 0.75g m^{-3} (Moore et al., 1999) and represents an operational product of the Coastal GMES Service Element Coastwatch. Black Sea Coastwatch data were further used here for inter-comparisons of model versus observations (see further in text).

3 Results

3.1 Horizontal circulation

The realism of the numerical simulation of circulation has been analysed in details by Grayek et al. (2010) thus only a brief overview is presented in this paper. The simulated currents (figure 8) agree with previous simulations based on different models (Staneva et al., 2001; Stanev et al., 2003). They reveal a dominating cyclonic pattern (figure 8a) that weakens during spring and summer (figure 8c, d). The latter is exemplified in figure 8c, d by the change of the sign of anomaly-circulation (clockwise). The anomaly displays cyclonic sense of rotation in winter (figure 8b),

that is the Rim Current gets stronger. The range of the winter-to summer change in the intensity of circulation is about the half of the annual mean value. The preliminary expectation is that this type of circulation will support a counter-clockwise transport of SPM.

3.2 Bed shear stress

Sediment dynamics was dominated by the distribution of sources and transport processes. The bottom acted as a source or sink depending on whether τ_b was larger or smaller than τ_{crit}. Therefore, it is instructive to consider the temporal and spatial characteristics of τ_b. The annual mean patterns of τ_b^c and τ_b^w demonstrated that both constituents of the bed shear stress have maxima in the coastal area (figure 9a,b). Over most of the bottom area that is in the deep ocean, the bed shear stress was more than one order of magnitude smaller than the averaged shelf value. Large values of τ_b^c along the western and southern coast were found in the embayment and headlands (e. g. Cape Kaliakra), while bed stress along the Caucasian coast was estimated to be extremely small, which is explained by the steep bottom and absence of pronounced headlands and embayments. Overall, figure 9c gives an idea about areas where the annual mean $\tau_b > \tau_{crit} = 0.02N/m^2$, that is areas favourable for erosion.

The temporal variability of the bed shear stress induced by wind waves τ_b^w (not shown here) follows the temporal variability of the wind-wave forcing (figure 7c), larger values are computed in winter and smaller ones in summer. It is important to mention that the action of the wind waves is relatively shallow and decreases rapidly with increasing ocean depth. The bed shear stress due to currents τ_b^c has a distinct seasonal cycle. During the intensification of the Rim Current in the autumn and winter τ_b^c reached the critical values all along the western coast.

More detailed analysis showed that there is no clear correlation between wind forcing (not the wind-wave one) and bottom friction. It appears that the increased values of bottom friction due to currents are a result of the eddy variability. The episodes of extreme τ_b^c that drive sediment erosion were explained by the events in the ocean weather, not the atmospheric weather.

3.3 Temporal variability

Temporal variability simulated in CSE and FSE is displayed in figure 10 for area mean concentrations and concentrations on the shelf and in the open sea (see figure 1 for the positions). In both runs area mean concentration was dominated by the high concentrations in the near coastal locations, therefore the black curve is above the green one. Coarse SPM reached lower concentrations because much of it deposited rapidly on the bottom.

In both runs maximum concentrations were observed during winter months, identifying the clear response of sediment system to atmospheric forcing. The signal was much smoother for the fine sediment (compare figure 10a and figure 10b), which is explained by the fact that small sinking velocities keep SPM longer in the suspension. In the case of coarse sediment shallow depths and large sinking velocities led to a removal of SPM from the suspension very rapidly therefore the oscillations were more pronounced and directly linked to the atmospheric forcing. Oscillations tend to decrease in magnitude with the increasing depth (compare the green and black lines in figure 10a).

The shape of the SPM curves in the sampled locations (figure 10c,d,e,f) differs significantly from the area mean ones - the deeper layers in most cases displayed also larger concentrations as compared to the sea surface. This is consistent with the fact that sediment settled and propagated mainly by advection. We have to denote that the surface maxima in the shelf point (figure 10c) is caused by direct transport from the Danube river because of particular circulation conditions. At the same time higher concentrations at 50m in the open sea were not due to local sources (if any they are deep below sea surface).

One interesting phenomenon displayed by the numerical simulations deserves to be mentioned. There were short time intervals in January, February and December, during which the two sediment curves overlapped. This could be considered as an indication of the role of convection homogenising rapidly the water column (figure 10c,e). This could have shaped SPM stratification and transport. This situation seems very "exotic" because, if the examined process occurs in realistic systems it has to work against settling, that is mixing associated with convective instability, could bring SPM up to the sea surface.

One last conclusion from figure 10f needs also to be made: in the open ocean area,

concentration of coarse SPM was negligible, that is this fraction sunk so rapidly in the coastal zone that it could not be found in the surface layers of ocean interior. On the contrary, the light sediment transported by advection is still in suspension in the open sea (figure 10e).

3.4 Horizontal sediment patterns. Comparison between simulations and observations

3.4.1 Observations

In the following we describe six scenes for 2007, which we sampled from reliable data of more than 400 relatively cloud-free images. The sampling criterion included as much as possible cover, larger diversity in the spatial characteristics of meso-scale features, clear agreement or disagreement with numerical simulations. For convenience the data from Azov sea was masked because of extremely high concentrations of SPM from biogenic origin.

The major source of sediment was observed in the area of the north western shelf (figure 11a, c, e, f). The region with largest values was in a close proximity of the Danube Delta. From there the sediment plume propagated in most cases to the south along the Romanian and Bulgarian coasts and tended to form small-scale "fingers" (figure 11c, f) about 10-20 km long and 2 km wide. These "fingers" identified the area of origin of high concentration, which extended in some cases far into the open ocean.

In some periods, as for instance during 21 July (figure 11e) the Danube plume turned to the North and high TSM values dominated the entire shelf area. In this case a very thin intrusion formed at the western coast of Crimea, penetrating very deep into the basin interior. Similar propagation feature (almost on the continental slope) was clearly seen in figure 11f separated from the rest of shelf water by a zone with lower concentration.

The second and third important areas of origin of TSM are south of the Kerch Strait (figure 11b) and North of the Turkish Coast (Cape Synop, figure 11c). As illustrated by the model, in these areas concentration increases as a consequences of a combination of atmospheric forcing and dominating meso-scale dynamics in the ocean. As seen in figure 11c, a chain of narrow intrusions propagated to the west

between the Rim Current and the coast.

TSM patterns allow tracing important elements of the Black Sea eddy/meso-scale variability. Larger eddies had scales of several tenths of kilometre (figure 11b) and the corresponding mushroom structures and intrusions reached scales of more than 100 km. The size of coastal waves on the Rim Current and eddies propagating between the Rim Current and the coast was clearly detectable as about 50-80 km (figure 11b, c). In some cases, as for instance in figure 11f headlands along the Asia Minor coast appeared to give the origin of very small scale scale eddies with increased TSM concentration.

3.4.2 Numerical simulations

Because we do not assimilate data we do not expect that the individual synoptic images from the model agree with observations that is the simulated eddies were not positioned at the same place and time as the observed ones. More important here is to discuss general characteristics of TSM, such as scales, types of patterns, sources and their impact on the spatial characteristics. Therefore we show in figure 12 several snapshots from the model, which illustrate its performance, in particular characteristic features comparable with the ones derived from the observations. We also admit that distinguishing between sediment of different origin (river, bottom, biology) is not easy, which could create problems in the inter-comparison.

The overall comparison between simulations and observations indicated that the model was still too coarse to resolve the small scales of 1-3 km, which dominated the near coastal dynamics of sediment. These features discussed above were sub-grid for our model.

Eddies formed coherent flow structures with dimensions similar to coastal embayments. They propagated through these embayments over time scale of days to weeks enabling the transport of suspended sediments over long distances. The consecutive snapshots from the model gave an overall idea of the magnitude of changes that could occur over only a few days.

There was a good agreement between observations and simulations, as this concerned the north-western shelf. This is the area where concentrations reached in the model local maximum at all times. The expected maximum in the Danube mouth observed by the satellite (figure 11a,c,f) was simulated also by the model(figure 12b,c,d,f).

Large-scale eddies, intrusions, mushroom-type patterns (figure 12a, c,d,f) resembled the observations (compare with figure 11e,f). Comparison between figure 12a and figure 11a could serve as an indication that the model also replicated the intrusions associated in the area east of Kerch Strait.

Figure 12f gives an idea of the evolution of coastal waves and formation of coastal eddies on the continental slope. Similar process has been earlier observed in the same area by Sur et al. (1996) in their analysis of satellite data. In the present model validation figure 12f gave the model analogue of the chain of eddies in figure 11c propagating in the area of the western Black Sea continental slope.

From figure 12c, d it becomes clear that the sediment source along the Asia Minor propagated in a similar way as in figure 11b,c,e, however fine scale zonal intrusions could not be resolved by the model. Simulated coastal eddies along Asia Minor coast similar to ones in figure 11b, c were however resolved in figure 12b, e. An eastward propagation of small scale coastal waves between Sakarya and Sinop (figure 12d) found also a support in the satellite data analysed in the past (Sur et al., 1996). A rapid sinking of the sediment coming from the rivers along the Asia Minor coast in the vicinity of the vertical continental slope, which was identified by the abrupt decrease of SPM (figure 11f) was also visible in the model simulations(figure 12c). However, a number of small scale features are missing in the simulations indicating the need to further increase model resolution.

It is noteworthy that depending on the local circulation in the easternmost part of the Black Sea, which is sometimes dominated by the so called Batumi eddy, the source of sediment from the Georgian Rivers propagated either to the north west (along the Caucasus coast, figure 12f) or to the south (figure 12a).

3.5 Sediment transport

3.5.1 Penetration of SPM into the basin interior. Vertical sediment patterns.

Sediment modelling provides a means of illustrating how matter from rivers or remobilized from the bottom may be redistributed. A number of studies (e. g. Lewis and Landing, 1991) claim that the intrusions from bottom represented a mechanism by which bottom water penetrates the basin interior (see also Konovalov et al., 2003).

So far, this issue has not been thoroughly addressed by the Black Sea numerical modelling. Our simulations clearly revealed traces of such intrusions (figure 13) by meso-scale eddies along the steep bottom.

Obviously, the model revealed the key mechanisms for transport and delivery of sediment from the shelf environments into the deep ocean. It mimicked aspects of long-term depositional pattern observed in Holocene stratigraphy (see Fig. 7 from Ross et al., 1978). Danube sediments travelled southward during a series of episodic transport events. However, their penetration into the basin interior appeared to be limited.

Figure 13 displays annual mean vertical sections of SPM along 31 E simulated in FSE and CSE after 3 years of integration (trends in the sediment model are not seen after 2 years of integration). The difference between these plots explains‘ the role of settling velocity for the penetration of SPM in the basin. In these two experiments the critical bed shear stress was always reached somewhere, thus the sediment sources were associated both with fluxes from rivers and remobilisation of bottom sediment under extreme events (providing extreme bed shear stress). For a relatively large settling velocity (CSE) the sediment plume near the ocean surface could not propagate far from the river mouths and beyond the continental slope. This means that the rapidly sinking sediment could only leave the coastal area in the deeper layers (figure 13b). This is indeed the case in the southern and eastern Black Sea, which lacks a continental shelf, therefore sediment from coastal area could could easily reach larger depths.

Differently from CSE, in FSE the coastal sediment laden water propagated on the shelf much farther into the direction of the continental slope. The specific balance between the horizontal transport from one side and settling from another enabled coastal intrusions of suspended sediment to reach the basin interior (compare figure 13a with figure 13b) building a layer with maximum concentrations at $\sim$ 200-300 m. The position of this maximum is explained by the fact that most of the coastal intrusions appear in the area of continental slope at about 200 m, that is where the Rim Current is usually observed. This finding is supported by the observations of Wakeham et al. (1991), as well as by the recent unpublished data collected in the frame of SESAME project (refhttp://www.sesame-ip.eu/).

In the Black Sea the steepness of the continental slope is extremely large, in particu-

lar in its southern and eastern parts, and the topographic control (JEBAR, Stanev, 1990), which tends to trap the jet over the continental slope weakens. As a consequence of this specificity (vertical wall) the instabilities of the Rim Current increase in magnitude (Stanev, 2005). As demonstrated in section 3.4 both observations and numerical simulations revealed long-reaching horizontal intrusions of coastal waters in the surface and intermediate layers caused by jets and coherent eddies, which played the major role in the propagation of SPM further into the open ocean.

3.5.2 Erosion and Deposition

The above discussion is extended below with the analysis of erosion and deposition of SPM (figure 14). As mentioned in the Introduction, existing data are not sufficient to reveal the spatial characteristics of deposition, therefore numerical simulations could shed more light on this issue.

The total bed shear stress τ_b (figure 9c) governing the process of resuspension was determining the horizontal pattern of the erosion rate (figure 14a) thus a maximum was found in the entire northwestern shelf and along the western coast. The low level of turbulence in the deep ocean disabled erosion below 160m.

Substantial differences in the deposition rates are identified in the various simulations. In CSE the coarse sediment was trapped near the mouths of the rivers and in the southwestern coastal zone. On the contrary, the fine sediment(figure 14b) had the ability to be transported far from the area of its origin and significant part of the Danube input settled down in the entire northwestern shelf and along the western coast.

3.6 River fluxes versus erosion from bottom

In the analyses done so far, no separation of responses to different forcing has been addressed. In order to get an idea of the relevant importance of river discharge and seabed resuspension, we carried out the following two experiments: (1) WCSE where the sediment fluxes from river mouths were disabled (figure 16a, c, e, g) and (2) RCSE where fluxes from rivers were enabled, but the forcing associated with the wind waves was disabled (figure 16b, d, f, h). The joint action of the two mechanisms was included in the CSE and the corresponding results are shown in figure 15b, d,

f, h, along with with a similar presentation of observations from satellites.
In the absence of the wind-wave forcing, the sediment remained very close to the river mouths, and the seasonal changes were less important. Little exception can be seen during the cold part of the year when the strong currents increase the bottom shear stress and erode sediment along the western coast.
Simulations in which the wind-wave forcing was enabled but sediment flux from rivers was disabled (figure 16a, c, e, g) were very similar to CSE in the fall and winter seasons, revealing again that the sediment patterns are highly dependent upon the atmospheric forcing and resulting bottom resuspension. However, the river runoff maintains the availability of sediments, which are transported from the shelf into the open ocean.
In this context the study of Wijsman et al. (1999) on the sediment characteristics and benthic activity on the northwestern Black Sea shelf is worth mentioning. Using in-situ observations with a focus on the the River Danube as a source of suspended solids to the continental shelf, these authors identified the following regions: (1) the area just in front of the Danube Delta (large discharge), (2) the northern part of the continental shelf where the majority of the Danube discharges are transported, and (3) the southern part of the continental shelf characterised by low sedimentation rates and low rates of benthic mineralisation. Analysis provided above supports this schematics, in particular as it concerns the area of low sedimentation: in the case of absence of resuspension (figure 16b, d, f, h) sediment concentrations are high only in front of the Danube Delta. South of the delta (along the Bulgarian coast) concentration of coarse sediment decreases substantially.

4 Conclusions

The modelling examples and data from remote sensing discussed in this paper demonstrated clearly the potential for the model to address the sediment dynamics in the Black Sea. We found that forcing due to wind waves provides the major driving element, which results from episodic high energy events contributing to the increase of horizontal sediment fluxes over the north-western shelf. Circulation and eddies shaped further the distribution of sediment. Comparison with observations was encouraging for the future use of this model.

The penetration of suspended sediment into the basin interior was shaped by the dynamics of coastal and open-ocean eddies. Fine sediment at sea surface could efficiently cross the continental slope and was observed at sea surface both in open-ocean observations and simulations in the form of coherent structures intrusions and wave-like patterns. On the opposite, coarser fractions sink rapidly along the bottom and can be observed over the continental slope and only below sea surface.

The patterns characterizing coarse and fine sediment are too different in the vertical plane. While the coarse sediment follows approximately the bottom, the fine one enters the deep ocean at about 200 m building a pronounced layer of maximum concentration in the basin interior. The plausibility of numerical simulations and interpretation of this result is supported by earlier local observations (Wakeham et al., 1991), as well as by recent surveys in the frame of SESAME activities.

Some unexpected results deserve also to be mentioned. It appeared that winter convection mixes SPM in the surface layer, and could provide an important mechanism for sediment transport. This mechanism identified by the numerical simulations needs to be validated against dedicated observations.

Numerical experiments with included or excluded different forcing terms, e. g. sediment flux from rivers appeared to be very useful enabling determine the spatial extensions of different point-sources. Analysis of numerical simulations supported earlier concepts of Wijsman et al. (1999) about sedimentation around of and south of the Danube Delta. Without resuspension mechanism in the model, sediment concentrations were high only in front of the Danube Delta. The continental shelf south of the delta (along the Bulgarian coast) was characterised by low concentration of coarse sediment and low rates of sedimentation.

Some future developments have to be performred in order to construct a realistic map of bottom sediment, which is needed to improve the bottom boundary condition. Once a map is available combining different type of sediments in a common system could provide more accurate information about the erosion process. Coupling the sediment transport model to ecosystem model (e. g. Gregoire and Beckers, 2004) will increase the realism and open the road to studying the light climate in this basin. Testing the model simulations against ship-based and moored instruments measurements of currents and sediment transport is also needed. Downscaling to scales on the order of 100 meters to permit adequate resolution of bottom topography

and complex shoreline has also to be tried.

ACKNOWLEDGEMENTS We are grateful to H. Guenther and G. Gayer for their help in setting up the WAM model for the Black Sea and useful discussions for tuning the sediment model. Useful comments and suggestions have been provided by J. Staneva and M. Gregoire. This study was supported by the EU-funded IP-s SESAME and ECOOP.

References

[1] Abdalla, S. and E. Ozhan, 1999. Wind and wave climate of the Mediterranean and the Black Sea Proceedings of the International MEDCOAST Conference 30 March - 2 April 1999, Antalya , Turkey, 404 p.

Balkas, T, G Dechev, R Mihnea, O Serbanescu, and U Unluata, 1990. State of the marine environment in the Black Sea region. UNEP Regional Seas Report and Studies 124, UNEP, 41 pp.

Barnier, B., G. Madec, T. Penduff, J.-M. Molines, A.-M. Treguier, J. L. Sommer, A. Beckmann, A. Biastoch, C. Boning, J. Dengg, C. Derval, E. Durand, S. Gulev, E. Remy, C. Talandier, S. Theetten, M. Maltrud, J. McClean, and B. D. Cuevas, 2006. Impact of partial steps and momentum advection schemes in a global ocean circulation model at eddy-permitting resolution. Ocean Dyn., doi : 10.1007/s10 236–006–0082–1.

Bevera, A. J., CK Harris, CR Sherwood, RP Signell (2009) Deposition and flux of sediment from the Po River, Italy: An idealized and wintertime numerical modelling study, Marine Geology, 260, Issues 1-4, Pages 69-80

Bondar, C, I State, D Cernea, and E Harabagiu, 1991. Water flow and sediment transport of the Danube at its outlet into the Black Sea. Meteorology and Hydrology 21, 21–25.

Brockmann, C., 2003, Demonstration of the BEAM software – a tutorial for making best use of VISAT. In Proceedings of the MERIS User Workshop, ESA ESRIN, Frascati, Italy, published on CD-Rom, ESA SP-549.

Cherneva, Z., Andreeva, N., Pilar, P., Valchev, N., Petrova, P. and Guerdes Coares, C, 2008. Validation of the WAMC4 wave model for the Black Sea, Coastal Engineering, 55, 11, 881-893.

Clarke, S, and AJ Elliott, 1998. Modelling suspended sediment concentration in the Firth of Forth. Estuarine, Coastal and Shelf Science 47, 235–250.

Doerffer, R and H Schiller, 1998. Pigment index, sediment and gelbstoff retrieval from directional water leaving radiance reflectances using inverse modelling technique. MERIS ATBD 2.12, Doc No. PO-TN-MEL-GS-0005

Doerffer R, Schiller H, Peters M, 2006. Meris regional case 2 water algorithms (c2r). www.brockmann-consult.de/beam/software/plugins/merisc2r-1.1

Gregoire M. and Beckers JM. Modeling the nitrogen cycle in an enclosed environment (the Black Sea) : transport versus biogeochemical processes and exchanges across the shelf break. Biogeosciences, 1(1), 30-61, 2004.

Griffies, S. M., 2004. Fundamentals of ocean climate models. Princeton University Press, 434pp.

Einstein HA, Krone RB (1962) Experiments to determine modes of cohesive sediment transport in salt water. J Geoph Res 67: 1451-1461

Gayer, G.; Dick, S.; Pleskachevsky, A.; Rosenthal, W.: Numerical modelling of suspended matter transport in the North Sea. In: Ocean Dynamics. Vol. 56 (2006) 62 - 77. (DOI: 10.1007/s10236-006-0070-5)

Ginsburg, AI, AG Kostianoy, DM Soloviev, and SV Stanichny, 1997. Coastal upwelling in the north-west Black Sea. Issledovaniya Zemli iz Kosmosa, 6, pp. 61–72(in Russian).

Giosan, L, JP Donnelly, E Vespremeanu, JP Bhattacharya, C Olariu, and F S Buonaiuto, 2005. River delta morphodynamics: Examples from Danube delta. In Giosan, L., and Bhattacharya, J.P. (Eds.), River Deltas: Concepts, Models and Examples, SEPM Special Publication, 85, 3-10.

Giosan, L, H. Bokuniewicz, N Panin, and J Postolache, 1999. Longshore sediment transport pattern along the Romanian Danube delta coast. Journal of Coastal Research 15:859-871.

GMES Service - Coastwatch Water Quality Monitoring Service, http://www.enviport.org/GMES/services/coastal/index.htm

Grant WD, and OS Madsen, 1979. Combined wave and current interaction with a rough bottom. Journal of Geophysical Research 84(C4):1797-1808.

Grayek, S, E. V. Stanev, and R. Kandilarov, 2010. On the response of Black Sea level to external forcing: Altimeter Data and Numerical Modelling. Ocean Dynamics, DOI 10.1007/s10236-009-0249-7.

Guneroglu, A, E Kose, F Karsli, M Feyzioglu, I Kurt, (2005) Maping and Comparison of Different Sensors' Geophysical Products in the Eastern Black Sea Region, MERIS and AATSR Workshop, European Space Agency (ESA), Frascati, Italy.

Günther, H., S. Hasselmann and P.A.E.M. Janssen, 1991. 'Wamodel cycle 4'. DKRZ report no. 4, Hamburg.

Harris, C. K., C. R. Sherwood, R. P. Signell, A. J. Bever, and J. C. Warner (2008), Sediment dispersal in the northwestern Adriatic Sea, J. Geophys. Res., 113, C11S03, doi:10.1029/2006JC003868.

Hay, BJ (1994). Sediment and water discharge rates of Turkish Black Sea rivers before and after hydropower dam constructions. Environmental Geology, 23, 276–283.

Hay, B J. and S Honjo (1989), Particle Deposition in the Present and Holocene Black Sea, Oceanography, 2(1), 26-31.

Honjo, S, S Kempe, VA Ittekot, E T. Degens, T Konuk and E Izdar, 1990. Interannual variablity in particle flux in the southwestern Black Sea. Deep-Sea Research, 37, 911-928.

Jaoshvili, S, 2003. The Rivers of the Black Sea (in Russian and English), Copenhagen, Denmark

Jonsson IG (1966) Wave boundary layers and friction factors. In: Proceedings of the 10th International Conference on Coastal Engineering, Tokyo, Japan, ASCE, pp 127-148

Kara, AB., AJ. Wallcraft, and H Hurlburt, 2005. A new solar radiation penetration scheme for use in ocean mixed layer studies: An application to the

Black Sea using a fine resolution Hybrid Coordinate Ocean Model (HYCOM). Journal of Physical Oceanography 35:13-32

Kara, A B., Wallcraft, A J. Hurlburt, H E. and E V Stanev (2008) Air–sea fluxes and river discharges in the Black Sea with a focus on the Danube and Bosphorus, 74 (2008) 74–95.

Karabashev, G S, Evdoshenko, M A and Sheberstov, S V(2006) Normalized radiance spectrum as a water exchange event diagnostic, International Journal of Remote Sensing,27:9,1775 — 1792

Konovalov, S K, GW Luther, III, GE Friederich, DB Nuzzio, BM Tebo, JW Murray, T Oguz, B Glazer, RE Trouwborst, B Clement, K J Murray, and AS Romanov. 2003. Lateral injection of oxygen with the Bosporus plume: Fingers of oxidising potential in the Black Sea. Limnology and Oceanography, 48(6):2369-2376

Kopelevich OV, Burenkov VI, Ershova SV et al. Application of SeaWiFS data for studying of bio-optical characteristics in the Barents, Black and Caspian Seas // Deep-Sea Res. II. 2004. V. 51. N 10–11. P. 1063–1091.

Kourafalou, VH, YG Savvidis, CG Koutitas and YN Krestenitis, 2004. Modeling studies on the processes that influence matter transfer on the Gulf of Thermaikos (NW Aegean Sea). Continental Shelf Research, 24, 203-222.

Lewis B. L. and W. M. Landing (1991) The biogeochemistry of manganese and iron in the Black Sea. Deep-Sea Research, 38. S773-S803

Ludwig W., Dumont E., Meybeck M., Heussner S. River discharges of water and nutrients to the Mediterranean and Black Sea: major drivers for ecosystem changes during past and future decades? Progress in Oceanography 2009;80:199-217. doi:10.1016/j.pocean.2009.02.001.

Madec, G, 2008 : NEMO ocean engine. Note du Pole de modelisation, Institut Pierre-Simon Laplace (IPSL), France, No 27, ISSN No 1288-1619, 217pp.

Mehta, A J (1988), Laboratory studies on cohesive sediment deposition and erosion, in Physical Processes in Estuaries, edited by J. Dronkers and W. van Leussen, pp. 327-345, Springer, New York.

Mikkelsen, O. A., P. S. Hill, and T. G. Milligan, 2007. Seasonal and spatial variation of floc size, settling velocity, and density on the Apennine margin (Italy). Continental Shelf Research, 27: 417-430.

Milligan, T. G., P. S. Hill and B. A. Law, 2007. Flocculation and the loss of sediment from river plumes. Continental Shelf Research, 27: 309-321.

Moore, GF, Aiken J., and Lavender, SJ 1999 The Atmospheric Correction of water colour and the quantitative retrieval of suspended particulate matter in Case II Waters: application to MERIS. MERIS Special Issue, International Journal of Remote Sensing, 20, 9, 1713-1733. [Abstract]

Morel, A and S Maritorena (2001): Bio-optical properties of oceanic waters: A reappraisal. Journal of Geophysical research, 106, 7763-7780.

Müller, G. and Stoffers, P., 1974. Mineralogy and petrology of Black Sea Basin sediments. In Degens, E.T. and Ross, D.A. (Eds.), The Black Sea geology, chemistry, and biology: Am. Assoc. Petrol. Geol. Mem. 20, p. 200-248.

Nikolov, H., E Trifonova, Z. Cherneva, R. Ostrowski, M. Skaja and M Szmytkiewicz (2006). Longshore sediment transport at Golden Sands (Bulgaria), Oceanologia, 48 (3), 2006. pp. 413-432.

Oguz, T, 2005. Black Sea ecosystem response to climatic variations. Oceanography, 18(2), 122-133

Panin N, 1996 Danube delta. Genesis, evolution, geological setting and sedimentology. Geo-Eco-Marina 1, 7–23.

Panin N, and D Jipa (2002) Danube River Sediment Input and its Interaction with the North-western Black Sea, Estuarine, Coastal and Shelf Science, 54, 551-562

Partheniades E (1965), Erosion and deposition of cohesive soils. *Journal of the Hydraulic Division*, ASCE, 91(HY1)

Peneva, E, E Stanev, V Belokopytov, and P-Y Le Traon (2001) Water transport in the Bosphorus Straits estimated from hydro-meteorological and altimeter data: seasonal to decadal variability. J. Mar. Sys. 31, 21-33.

Popa, A. 1993 Liquid and sediment inputs of the Danube River into the northwestern Black Sea. In Transport of Carbon and Nutrients in Lakes and Estuar-

ies, Part 6 (Kempe, S., Eisma, D. & Degens, E. T., eds). Mitteilungen aus dem Geologisch-Palaontologischen Institut und Museum der Universitat Hamburg, SCOPE/UNEP Sonderheft 74, 137–149.

Puls, W, and J Sündermann (1990), Simulation of suspended sediment dispersion in the North Sea, in Residual Currents and Long-Term Transport, vol. 38, Coastal and Estuarine Studies, edited by R. T. Cheng, pp. 356 – 372, Springer, New York.

Ross, D A, P Stoffers, and ES Trimonis, 1978. Black Sea Sedimentary Framework. Contribution 3970, Woods Hole Oceanographic Institution, Woods Hole, Massachusetts, doi:10.2973/dsdp.proc.42-2.106.1978

Roussenov, V, E Stanev, V Artale, and N Pinardi (1995), A seasonal model of the Mediterranean Sea general circulation, J. Geophys. Res., 100(C7), 13,515–13,538.

Sanford, L.P. and J.P.Y.Maa, 2001. A unified erosion formulation for fine sediments. Marine Geology, 179: 9-23.

Sherwood, CR, JW Book, S Carniel, L Cavaleri, J Chiggiato, H Das, J D Doyle, C K Harris, A W Niedoroda (2004) Sediment Dynamics in the Adriatic Sea Investigated with Coupled Models, Oceanography 17 (4), pp. 58–69.

Signell, R. P., R. C. Beardsley, H. C. Graber, and A. Capotondi (1990), Effect of wave-current interaction on wind-driven circulation in narrow, shallow embayments, Journal of Geophysical Research, 95(C6), 9671–9678.

Simonov, A I and E N Altman, Editors. 1991. Hydrometeorology and hydrochemistry of the USSR seas. Vol. IV, The Black Sea, Gidrometeoizdat, 430 pp.

Soulsby, R.L., 1997, Dynamics of Marine Sands, Thomas Telford Publications, London.

Stanev, E V, 1990. On the mechanisms of the Black Sea circulation. Earth-Science Reviews 28:285-319.

Stanev, E V (2005) Understanding Black Sea Dynamics: Overview of recent numerical modelling, Oceanography, Vol.18, No.2, 52-71.

Stanev, E V, J-M. Beckers, C Lancelot, JV Staneva, P-Y Le Traon, E L Peneva, and M Gregoire. 2002. Coastal-open ocean exchange in the Black Sea: Observations and modelling. Estuarine Coast and Shelf Science 54:601-620.

Stanev, E. V., M. J. Bowman, E. L. Peneva, and J. V. Staneva (2003) Control of Black Sea intermediate water mass formation by dynamics and topography: comparisons of numerical simulations, survey and satellite data. J. Mar. Res., 61,59-99.

Stanev EV, Brink-Spalink G, Wolff J-O (2007) Control of sediment dynamics by transport and turbulence. A case study for the East Frisian Wadden Sea. J Geoph Res 112, C04018, doi:10.1029/2005JC003045

Staneva, J. V., D. Dietrich, E. Stanev, and M. Bowman (2001) Rim current and coastal eddy mechanisms in an eddy-resolving Black Sea general circulation model. J. Mar. Sys. 3, 137-157

Staneva, J V., E V. Stanev, and N H Rachev (1995), Heat balance estimates using atmospheric analysis data: A case study for the Black Sea, J. Geophys. Res., 100(C9), 18,581–18,596.

Sur, HI, Ozsoy, E, Ilyin, YP and Unluata, U, 1996. Coastal/deep ocean interactions in the Black Sea and their ecological/environmental impacts. J. Marine Systems 7, pp. 293–320.

Traykovski P, WR Geyer, JD Irish, and JF Lynch. 2000. The role of wave-induced density-driven fluid mud flows for cross-shelf transport on the Eel River continental shelf. Continental Shelf Research 20:2113-2140.

Traykovski, P., P. L. Wiberg, and W. R. Geyer, 2007. Observations and modelling of wave supported sediment gravity flows on the Po prodelta and comparison to prior observations from the Eel shelf. Continental Shelf Research, 27: 375-399.

Ulses, C., C. Estournel, X. Durrieu de Madron and A. Palanques, 2008, Suspended sediment transport in the Gulf of Lions (NW Mediterranean): Impact of extreme storms and floods. Continental shelf research Continental Shelf Research 28, 2048–2070

Wakeham, SG, JA Beier, CH Clifford (1991) Organic matter sources in the Black Sea as inferred from hydrocarbon distributions. In I. Izdar and J. Murray (eds.), Black Sea Oceanography, 319-341.

WAMDI Group. The WAM model—a third generation ocean wave prediction model. Journal of Physics Oceanography 1988; 18:1775–1810.

Wang, X H, and N Pinardi (2002), Modeling the dynamics of sediment transport and resuspension in the northern Adriatic Sea, J. Geophys. Res., 107(C12), 3225, doi:10.1029/2001JC001303.

Wiberg, P.L., Drake, D.E. and Cacchione, D.A., 1994. Sediment resuspension and bed armoring during high bottom stress events on the northern California inner continental shelf: measurements and predictions. Continental Shelf Research, 14(10/11): 1191-1219.

Wijsman, JWM, Herman, PMJ, Gomoiu, M-T, (1999). Spatial distribution in sediment characteristics and benthic activity on the northwestern Black Sea shelf, Mar Ecol Prog Ser, 181, 25-39.

Winguth, C, Wong, HK, Panin, N, Dinu, C, Georgescu, P, Ungureanu, G, Krugliakov, VV and Podshuveit, V, 2000. Upper Quaternary water level history and sedimentation in the northwestern Black Sea. Marine Geology, 167(1-2): 127-146.

5 Figures

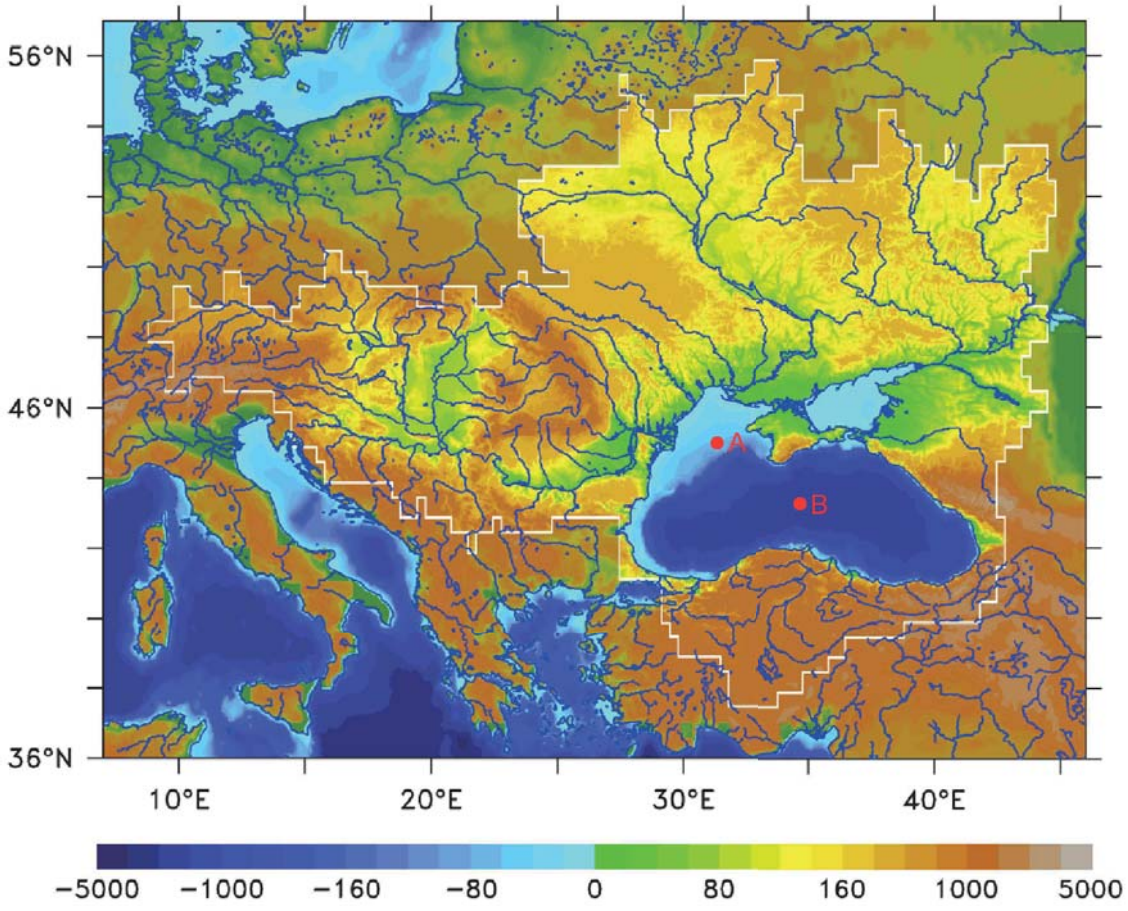

Figure 1: The Black Sea and its catchment area. Orography of the catchment area (m) is plotted with brighter colours. Bottom topography (m) is coloured in blue, shelf in light blue, deep-ocean in dark blue. Note that shelf is almost absent in the southern and eastern parts of the sea. Positions of locations discussed further in the paper are also shown.

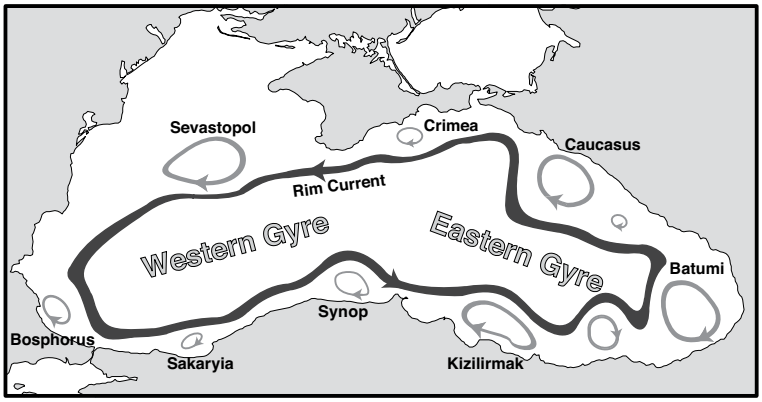

Figure 2: Black Sea circulation (presented schematically based on numerical simulations of Stanev, 2005). The names of major coastal eddies as known from observations (usually, associated with geographic names, for example, capes and towns) are also given.

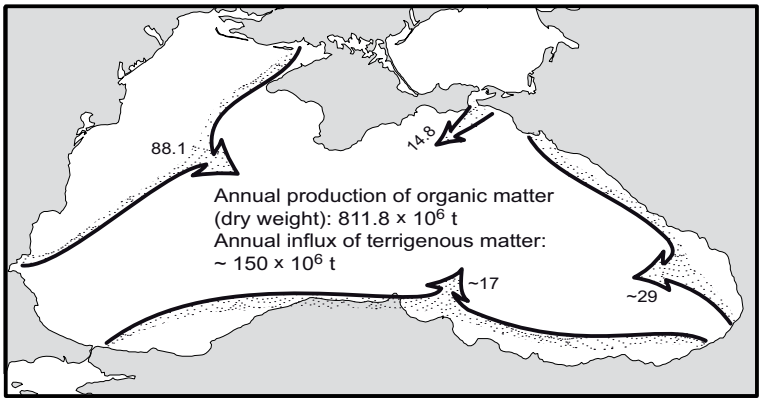

Figure 3: Supply of sedimentary material (in 10^6 t/yr) into the Black Sea interior (replotted from Shimkus and Trimonis, 1974).

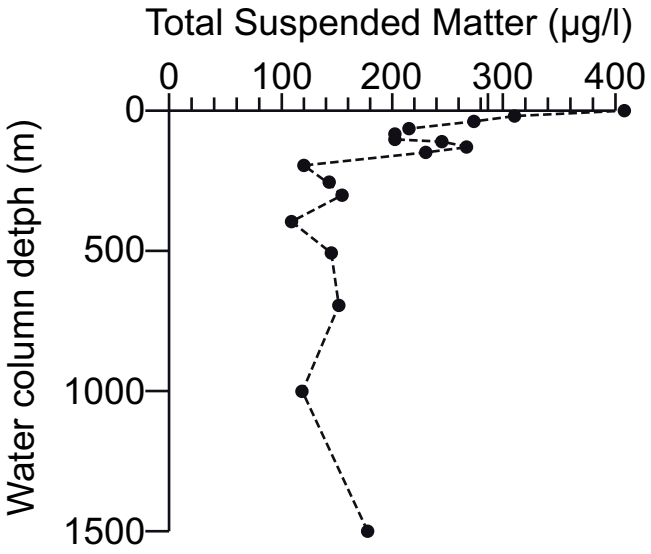

Figure 4: Vertical distribution of TSM (redrawn from Wakeham et al., 1991).

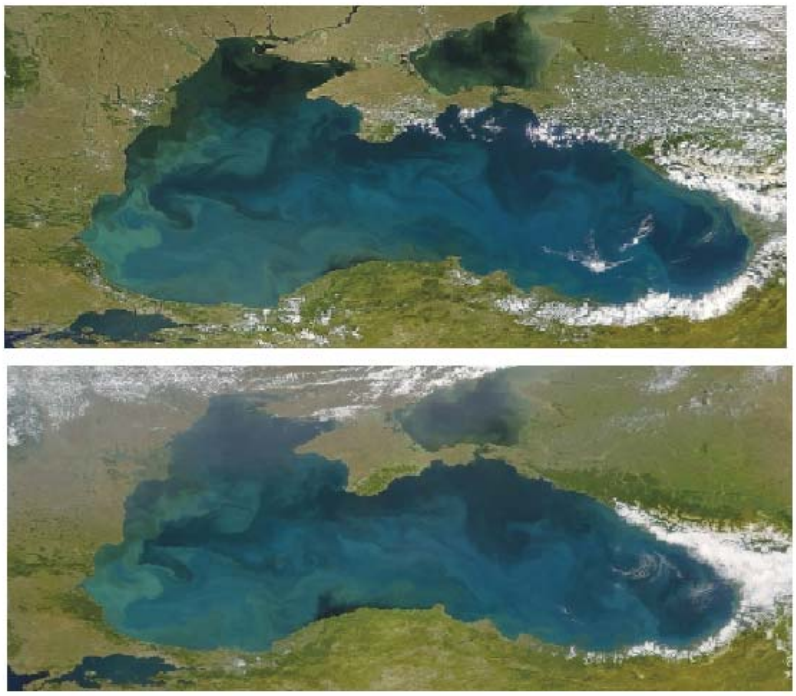

Figure 5: This image has been provided by SeaWiFS Project, NASA/Goddard Space Flight Center and ORBIMAGE and shows the surface patterns of the Black Sea turbid waters on June 11 (uper panel) and June 13 2000 (bottom panel).

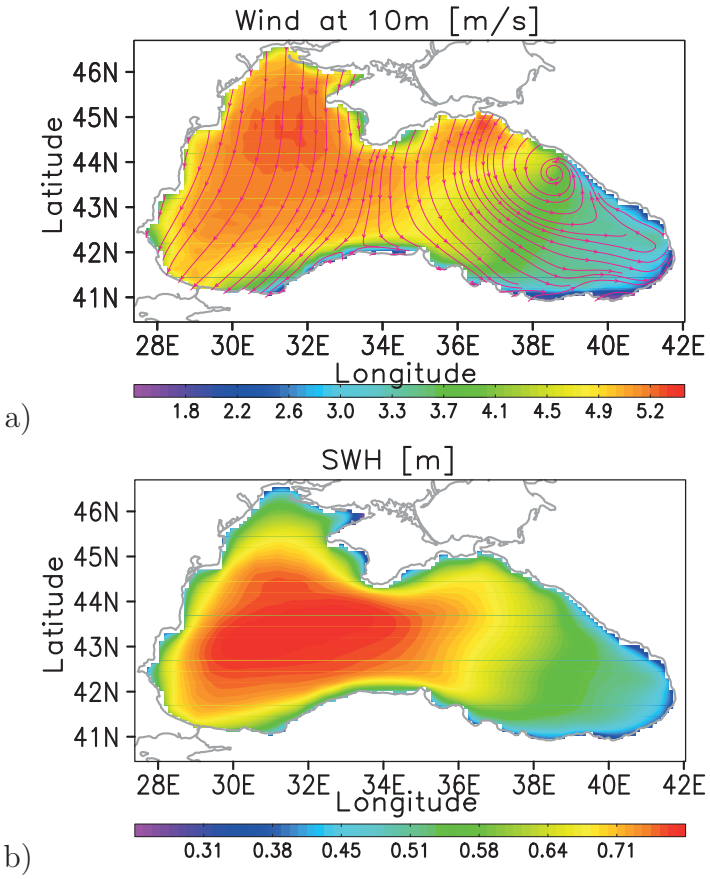

Figure 6: Annual mean wind (a) and significant wave height(SWH) forcing (b).

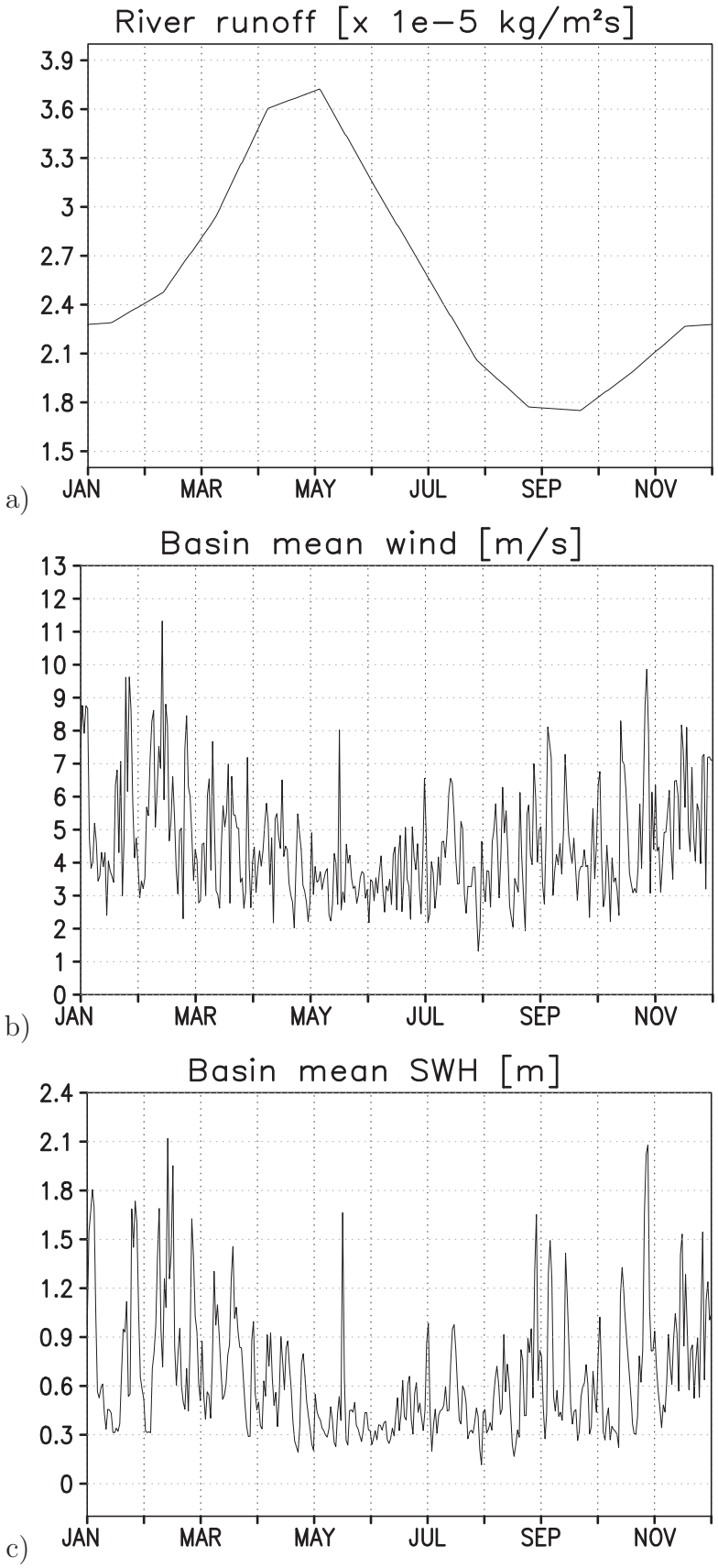

Figure 7: Temporal variability of the river runoff (a), basin mean wind (b), and basin mean significant wave height (SWH) (c).

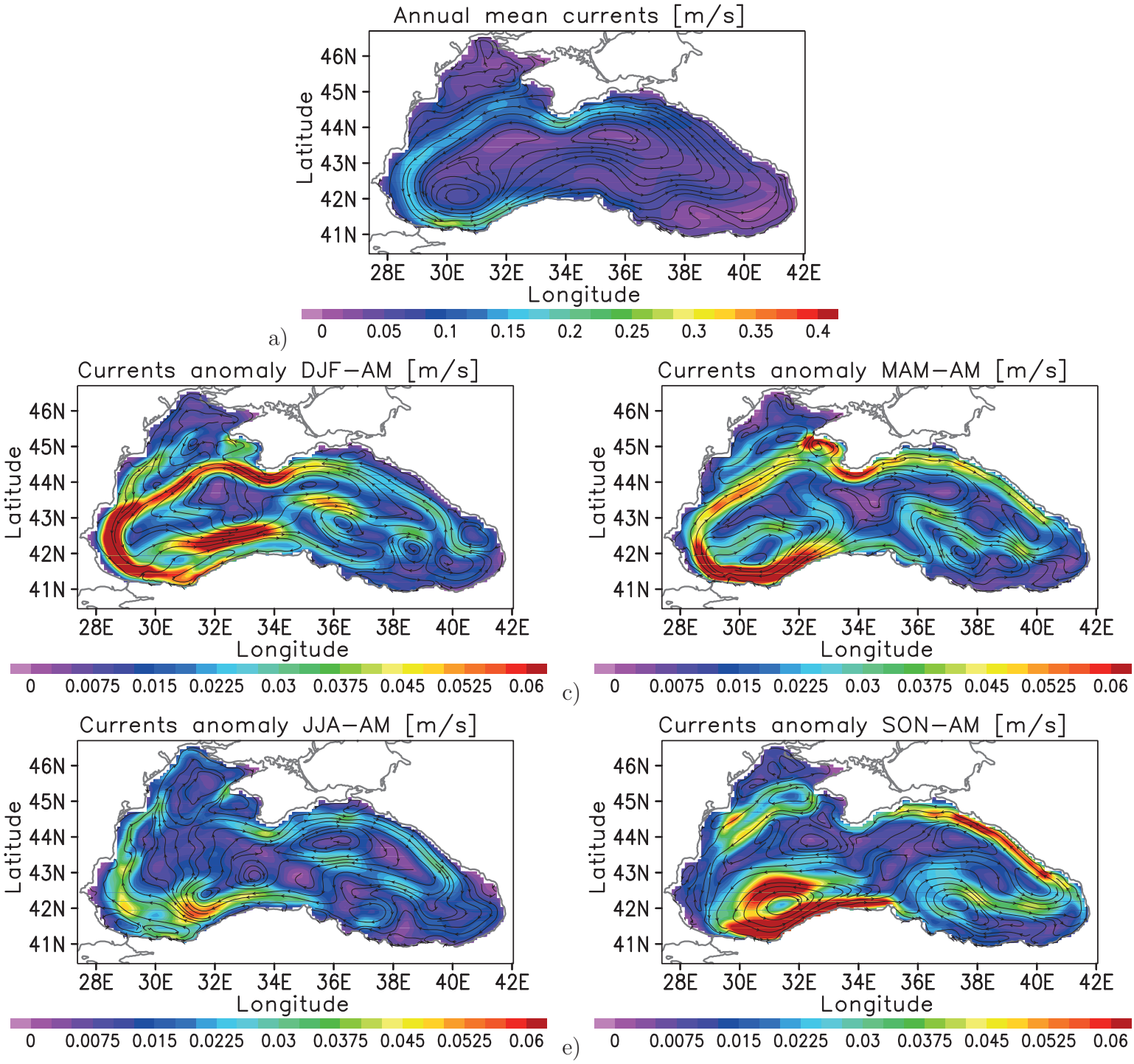

Figure 8: Simulated annual mean (a) and anomalies of the seasonal mean (b-e) surface currents.

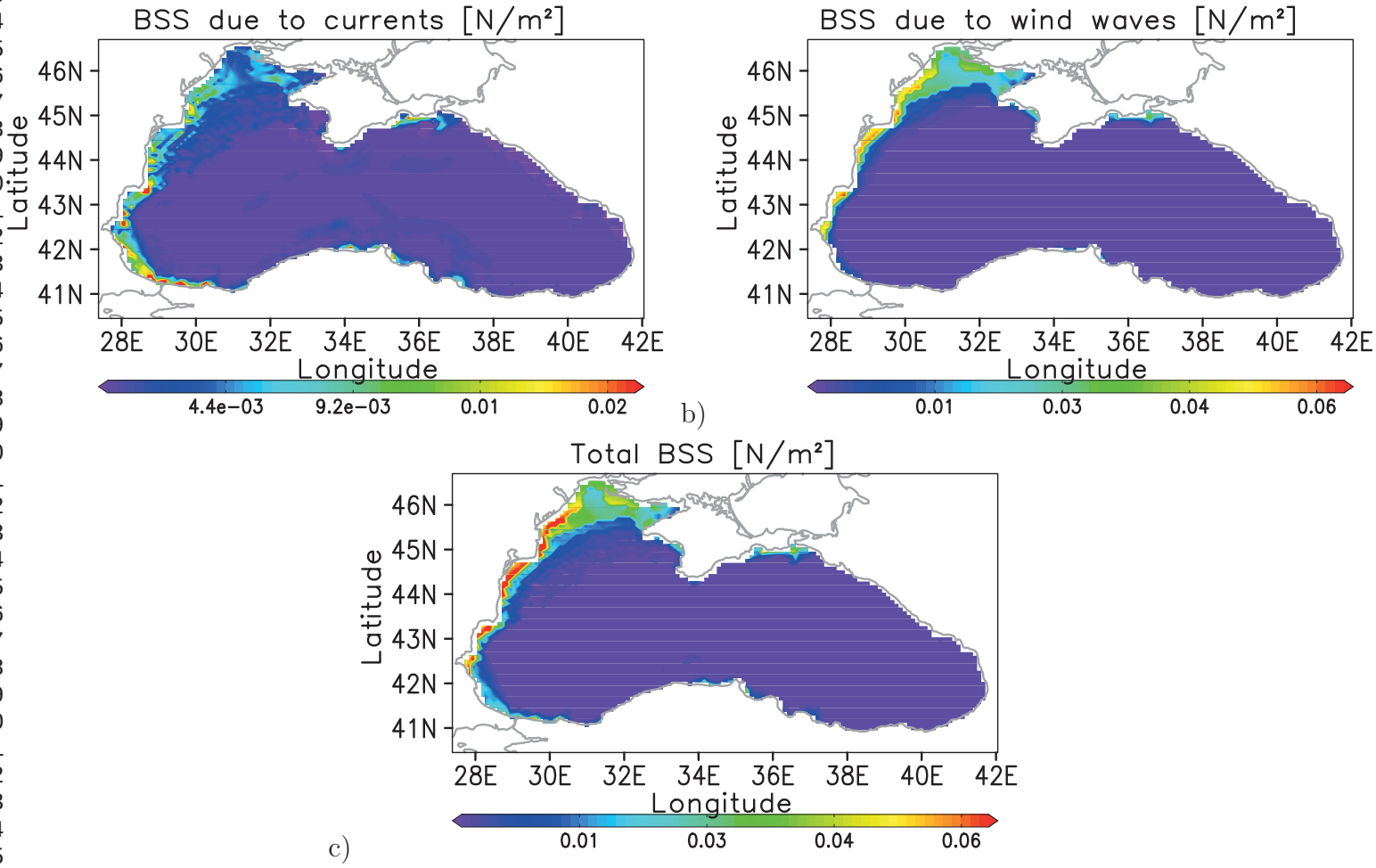

Figure 9: Annual mean bed shear stress (BSS) due to currents (a), wind waves (b) and combined (c)

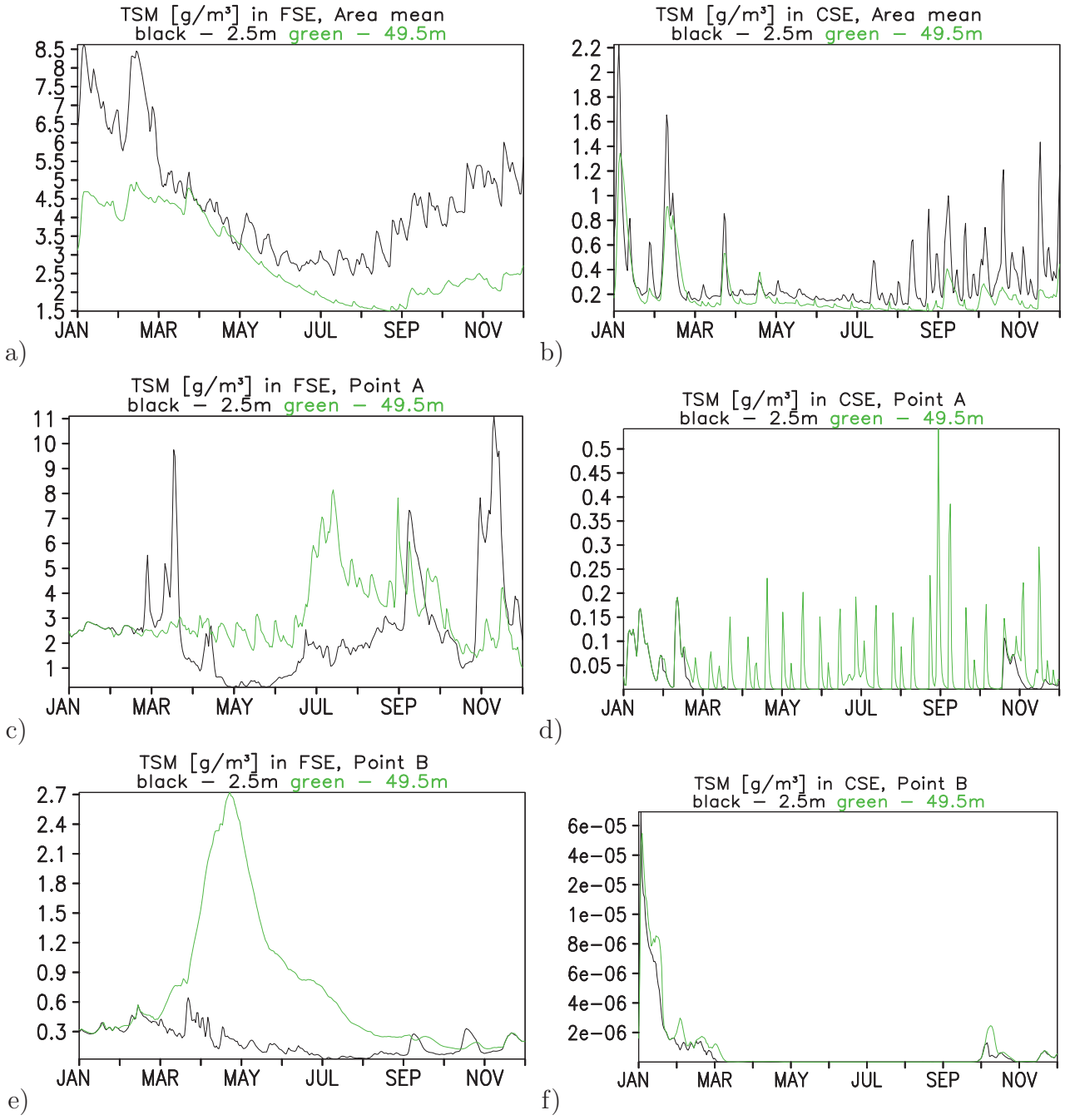

Figure 10: Temporal evolution of surface TSM (black line) and TSM at 49.5 m (green line) in FSE (a, b, c) and CSE (d, e, f). Basin mean concentration (a,d) as well as local concentration in the area of north-western shelf (Point A, 45.0N,31.0E, b, e) and open sea (Point B, 43.3N, 34.3E, c, f) are presented. For the position of the locations see figure 1.

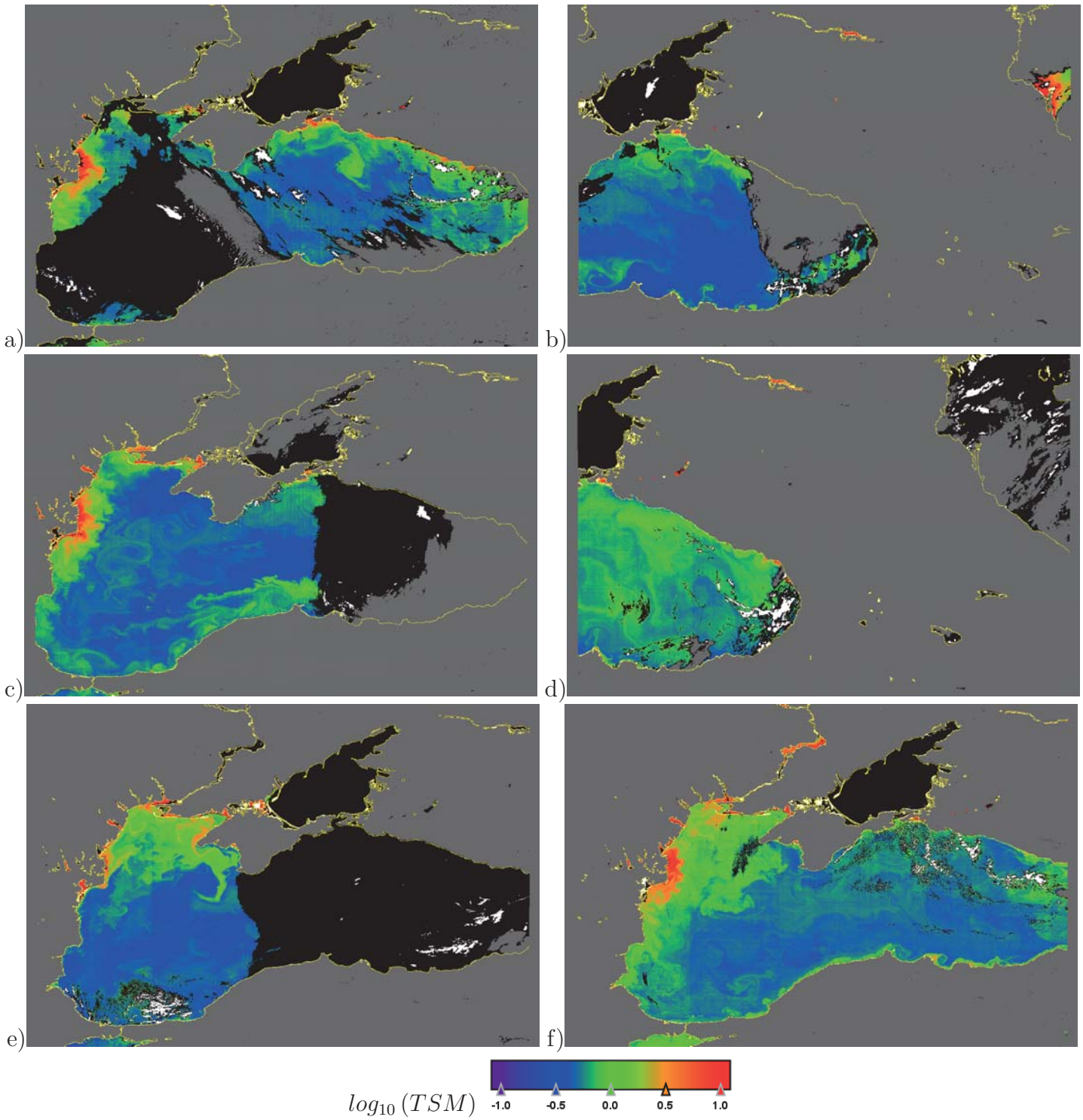

Figure 11: Surface TSM concentration from MERIS satellite in 2007 on 19.Mar. - a, 11.Apr. - b, 23.Apr - c, 03.Jul. - d, 21.Jul. - e, 18.Oct. - f

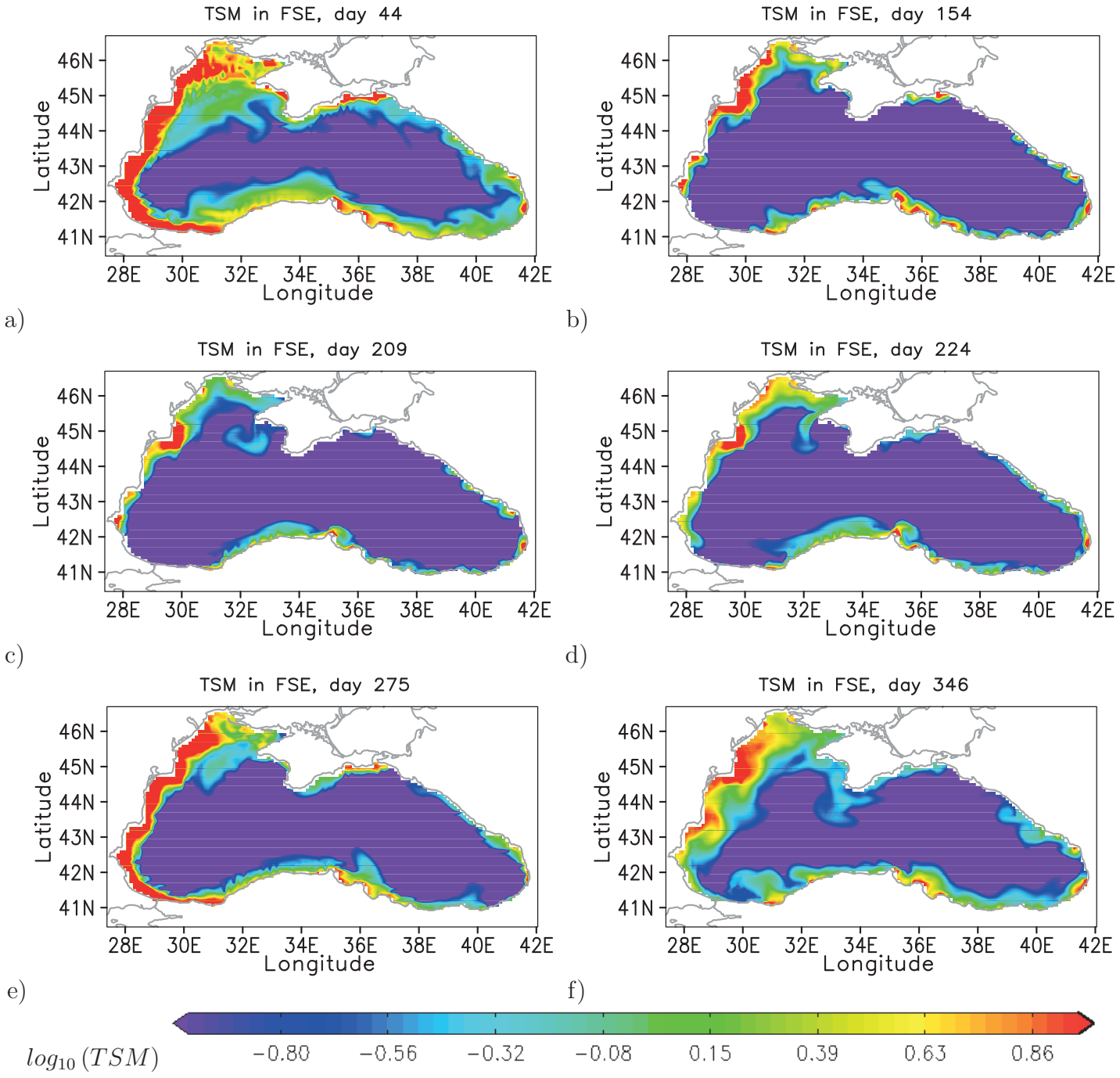

Figure 12: Surface TSM concentration as simulated in FSE in 2008 on 13.Feb. - a, 02.Jun. - b, 27.Jul. - c, 11.Aug. - d, 01.Oct. -e, 11.Dec. - f

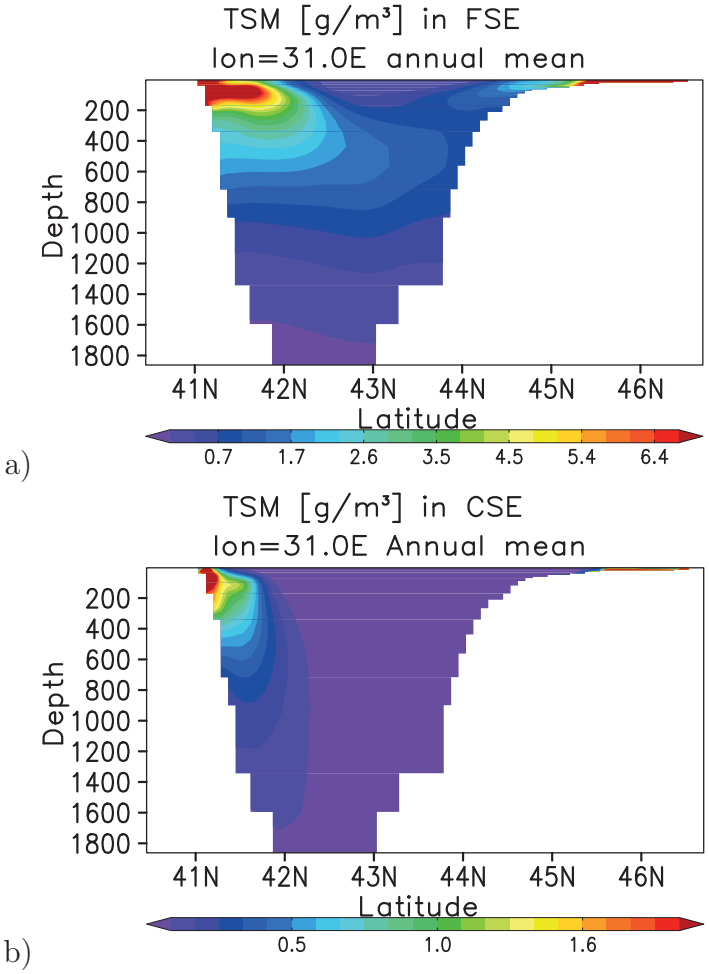

Figure 13: Vertical cross-sections of TSM at 31.0E as simulated in FSE - a) and CSE - b).

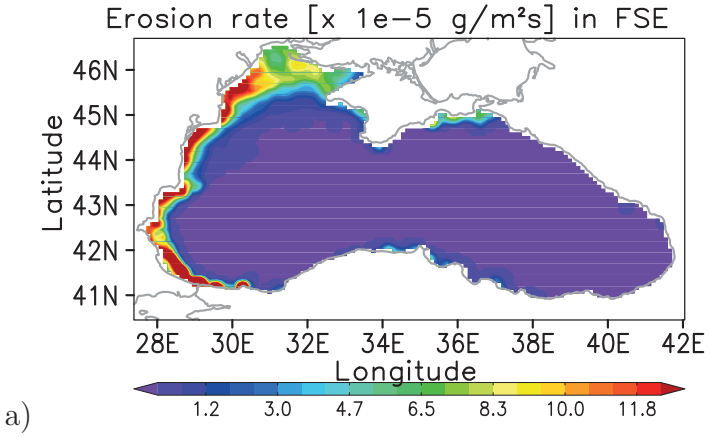

a)

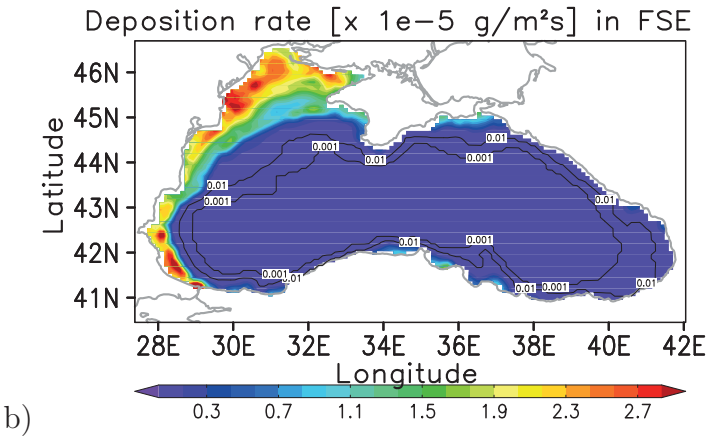

b)

Figure 14: Annual mean erosion rate (a) and annual mean deposition rate (b) and as simulated in FSE.

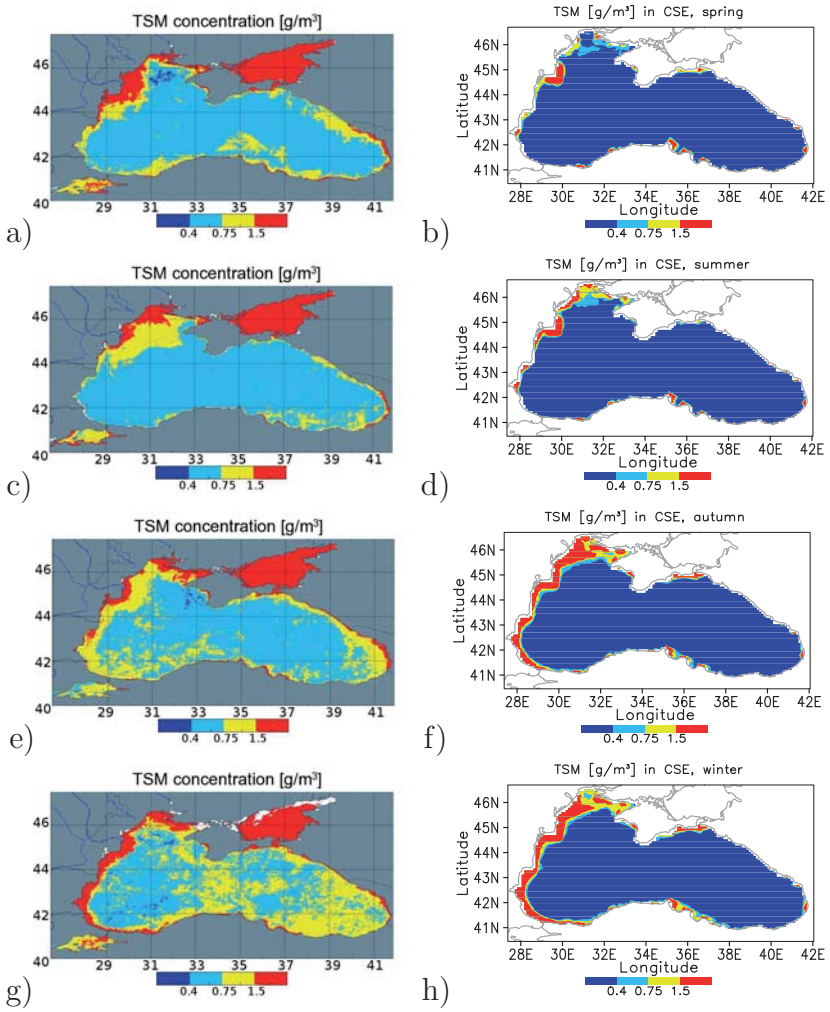

Figure 15: Seasonally averaged remote sensing TSM concentrations processed by ACRI ST(left column: a, c, e, and g) and model simulated seasonal mean TSM concentrations as in CSE (right column: b, d, f, and h). First row is spring, second one is summer, third one is fall, the last one is winter.

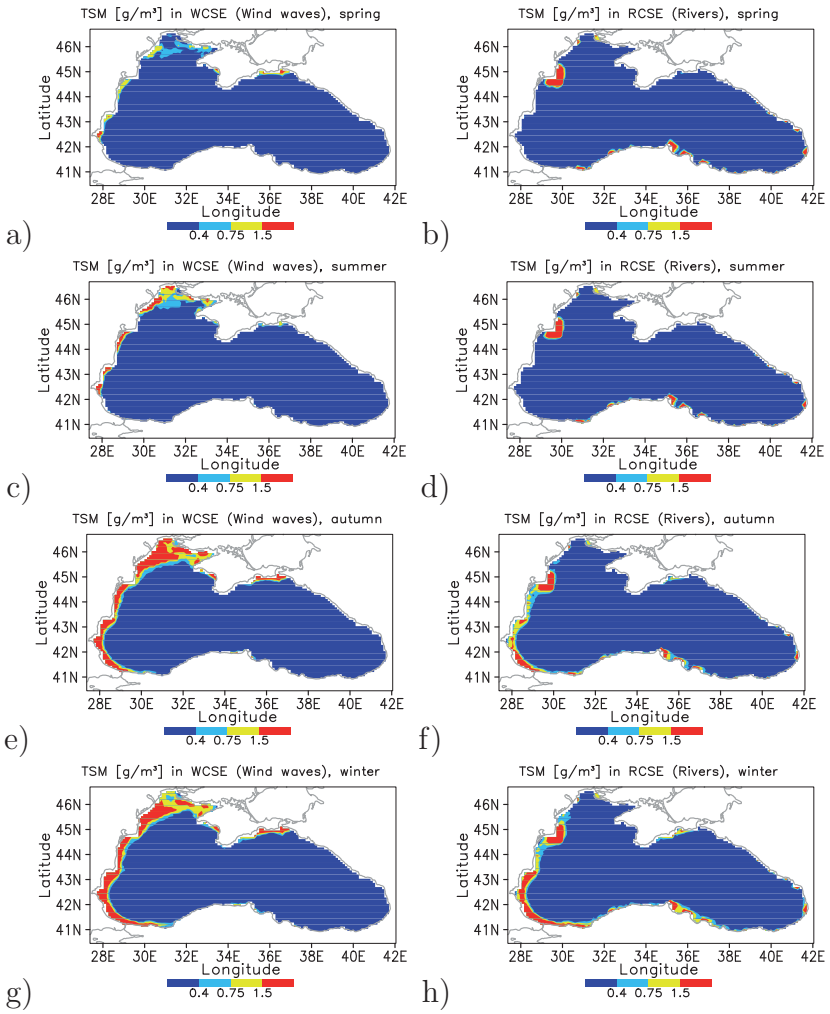

Figure 16: The impact of river and wind-wave forcing. Seasonally averaged TSM concentrations as simulated in WCSE and RCSE. The first column - WCSE(a, c, e, and g) corresponds to experiment with no river forcing (no sediment flux in the river mouth). In the second column - RCSE (b, d, f and h) the wind wave forcing has been neglected.